J. Plasma Phys. (2015), *vol.* 81, 905810609 © Cambridge University Press 2015
doi:10.1017/S0022377815001403

Plasma stability theory including the resistive wall effects

V. D. Pustovitov[1,2,†]

[1]National Research Centre 'Kurchatov Institute', Kurchatov Sq., 1, Moscow 123182, Russian Federation

[2]National Research Nuclear University MEPhI (Moscow Engineering Physics Institute), Moscow 115409, Russian Federation

(Received 13 July 2015; revised 16 November 2015; accepted 19 November 2015)

Plasma stabilization due to a nearby conducting wall can provide access to better performance in some scenarios in tokamaks. This was proved by experiments with an essential gain in β and demonstrated as a long-lasting effect at sufficiently fast plasma rotation in the DIII-D tokamak (see, for example, Strait *et al.*, *Nucl. Fusion*, vol. 43, 2003, pp. 430–440). The rotational stabilization is the central topic of this review, though eventually the mode rotation gains significance. The analysis is based on the first-principle equations describing the energy balance with dissipation in the resistive wall. The method emphasizes derivation of the dispersion relations for the modes which are faster than the conventional resistive wall modes, but slower than the ideal magnetohydrodynamics modes. Both the standard thin wall and ideal-wall approximations are not valid in this range. Here, these are replaced by an approach incorporating the skin effect in the wall. This new element in the stability theory makes the energy sink a nonlinear function of the complex growth rate. An important consequence is that a mode rotating above a critical level can provide a damping effect sufficient for instability suppression. Estimates are given and applications are discussed.

1. Introduction

In tokamaks and stellarators, plasma instabilities limit β (the ratio of the plasma pressure to the magnetic field pressure) to a level of several per cent. The related physics has been studied from the very beginning of fusion research, but still many issues remain unresolved [1, 2]. This field became a large science with dozens of publications appearing every month in journals and conference proceedings. In theory, it extends from the well-known general academic approaches [3–8] to elucidations of particular details [1, 2, 9]. Any attempt to review this area of knowledge is doomed to be fragmentary in both physics and references. Here, we discuss only several from the list of the most urgent problems of ITER [1, 2], which is currently the largest fusion project with a great impact on national programs worldwide. Briefly, wall stabilization is the central topic. Originally this was included in stability calculations by assuming that the vacuum vessel wall is an ideal

† Email address for correspondence: Pustovitov_VD@nrcki.ru

https://doi.org/10.1017/S0022377815001403 Published online by Cambridge University Press

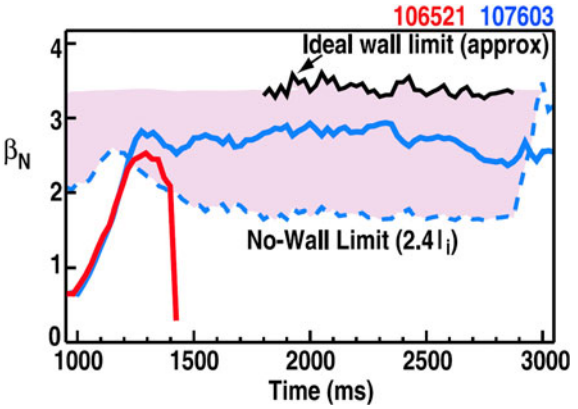


FIGURE 1. β significantly above the no-wall kink-mode stability limit is sustained for ~1.5 s (blue) with a resistive wall and plasma rotation in DIII-D. A similar discharge (red) without sufficient rotation has a β collapse soon after crossing the no-wall limit. (Figure 1 from [12].)

conductor [3–9]. Lately, attention has shifted to a more realistic analysis with a resistive wall, though the theory has been developed for very slow modes only.

The problem is known because of resistive wall mode (RWM) studies [1, 2, 10] with DIII-D tokamak as the main contributor of experimental results [10–25]. Its solution is needed to reach the ITER [1, 2] and JT-60SA [26, 27] goals because, if not stabilized, the RWMs can be a serious danger in advanced scenarios.

Among the DIII-D results, the most impressive, and still theoretically unexplained [2, 10], is the rotational stabilization of RWMs [10–25]. Its simple description is that stable operation significantly above the free-boundary ideal kink-mode β limit is possible with a resistive wall and sufficient plasma rotation [12]. This is illustrated by figure 1, showing a long pulse with high β in the DIII-D. The demonstrated gain in β makes such discharges an attractive option, but without a reliable predictive model, its extrapolation to ITER is problematic [1, 2, 10].

The effect is robust and reproducible; it was also observed on the tokamaks JET [21], NSTX [21, 28, 29], JT-60U [30] and several other devices [10]. However, it still remains a mystery [2, 10]. Simple theoretical estimates show that, in the frame of ideal magnetohydrodynamics (MHD), the RWMs cannot be stabilized by the plasma rotation [31–34]. At the same time, there is a contrary opinion that, when the mode rotates fast enough, the resistive wall must behave like an ideal conductor and stabilize the mode [1, 12, 17, 23, 35–40]. The experimental results, however, fall in between [10–25, 28–30]. Also, the concepts of 'fast enough' rotation and transition from the resistive to superconducting reaction were not clarified in fusion theory.

Analysis of the RWM stability in the non-rotating plasma is often performed in the frame of ideal MHD [1, 2, 10–25, 28–30, 35, 38, 41–49]. The stabilizing effect of the rotation was shown in the models with dissipation [10, 14, 16, 23, 25, 32, 36, 50–64] that treated the resistive wall as a magneto-thin shell, disregarding the skin effect. This can be justified for slow evolution, but at faster rotations, the skin effect makes the wall reaction nonlinear, which affects the energy exchange and may essentially contribute to stabilization [65–67].

Incorporation of the skin effect in the wall into the RWM theory is a key point here. Mathematically, this requires a proper description of the plasma–wall electromagnetic

https://doi.org/10.1017/S0022377815001403 Published online by Cambridge University Press

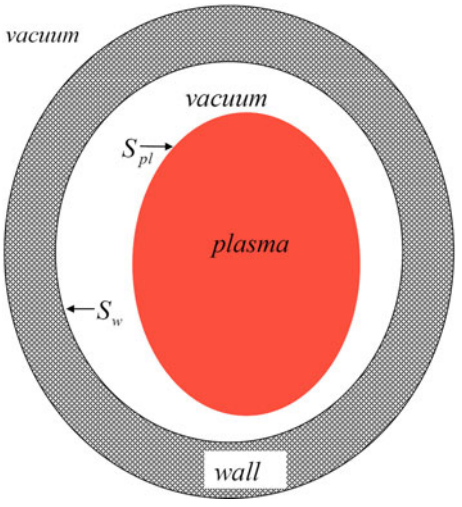


FIGURE 2. A schematic view of the perpendicular cross-section of the toroidal plasma separated from the wall by the vacuum gap. The plasma surface and inner surface of the wall are denoted as S_{pl} and S_w, respectively.

interaction which is governed by the Maxwell equations and Ohm's law for the resistive walls and can be coupled to the plasma by proper boundary conditions. In solving the outer task, we do not impose any constraint on the plasma model. This allows applications with only those minimal assumptions that are obviously needed for the coupling. For example, in some cases, it suffices to assume a linear plasma response to external perturbations instead of detailed specification of the plasma dynamics.

Theoretically, taking account of the skin effect is a step ahead of the traditional thin-wall approaches. Practically, this gives a tool for closer analysis of the events when the plasma generates a rotating perturbation.

The paper contains derivations based on the integral energy–torque balance, reductions of the general relations to simpler forms, stability analysis for the modes faster than conventional RWMs, estimates and discussion of theoretical and experimental results on RWMs and other phenomena where the resistive wall can affect the plasma stability.

2. Formulation of the problem

The configuration of interest is schematically shown in figure 2. A toroidal plasma is separated from the metal wall by a vacuum gap, and there is a vacuum behind the wall. In real tokamaks and stellarators, the walls are non-uniform with cuts, portholes, extensions, etc. This is carefully modelled in such codes as VALEN [41], STARWALL [68] or CarMa [69–71]. Also, behind the first wall there can be other conductors. For example, the ITER design is better reproduced by a double wall [2, 72], and the JT-60SA vacuum vessel will also have a double-wall structure [27]. Here such complications will not be discussed because, to begin with, we need a theory properly treating the nearest wall. The principal question here is whether or not the wall can only slow down the mode growth rate (compared to the 'no-wall' case) without other influences on the plasma stability. The latter viewpoint dominates in the RWM studies [1, 2, 10–16, 18, 20–25, 29–37, 40–46, 50, 52, 57–64, 68, 73].

https://doi.org/10.1017/S0022377815001403 Published online by Cambridge University Press

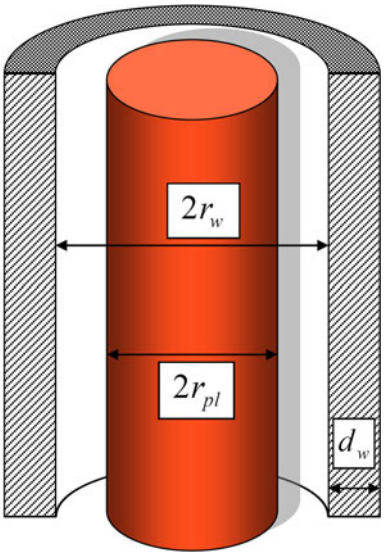


FIGURE 3. A cylindrical illustration of the task geometry. Plasma with radius r_{pl} and a coaxial resistive wall with radius r_w, uniform thickness d_w and electrical conductivity σ.

It is supported by the theorem proved for a dissipationless plasma in the paper [74], which compels us to look for some dissipation inside the plasma [10, 14, 16, 23, 25, 32, 36, 50–64] as a reason for higher stability limits due to the rotational stabilization. Recently developed and quite intricate theories with kinetic models [25, 55–64] include the wall as a thin shell, completely disregarding the skin effect. Here, on the contrary, we mostly concentrate on the cases when this effect becomes noticeable.

Some estimates will be performed using the cylindrical model which is also convenient for introducing the main geometrical parameters. The wall minor radius and the wall thickness are characterized by typical dimensions r_w and d_w, as shown in figure 3. In tokamaks, stellarators and pinches, the walls are geometrically thin, $r_w \gg d_w$. This, and the notion that the RWMs are slow modes [1, 2, 10–25, 29–46, 49–64, 68–73, 75], gave rise to so-called thin-wall approximation [2, 10, 13, 14, 16, 25, 35, 41–43, 46, 49, 53–64, 68, 73, 76–79] in the RWM theory that assumes the normal component of the magnetic perturbation to be constant across the wall. This requires $s \gg d_w$, where s is the skin depth in the wall. We are going to compare the predictions of such models with the results obtained for faster modes when $s \ll d_w$ and the same wall becomes magnetically thick.

The real perturbed quantities will be represented as

$$f(\boldsymbol{r}, t) = \mathrm{Re}\{f_1(\boldsymbol{r})\mathrm{e}^{\gamma t}\} \tag{2.1}$$

with complex growth rate

$$\gamma = \gamma_R + \mathrm{i}\gamma_I, \tag{2.2}$$

where the real γ_R and $\gamma_I = n\omega$ are the real growth rate and n-fold frequency of the mode toroidal rotation and n is the toroidal wavenumber. For estimates, when it is justified, we will use a simple cylindrical representation

$$f_1 = f_{1m} \exp \mathrm{i}(m\theta - n\zeta), \tag{2.3}$$

where θ and ζ are the poloidal and toroidal angles, and f_{1m} is the amplitude.

https://doi.org/10.1017/S0022377815001403 Published online by Cambridge University Press

The plasma stability is often analysed in the frame of the ideal MHD, which seems to be insufficient [2, 10, 14–20, 29, 55] for treating the rotational stabilization of RWMs. The ideal MHD is, however, a well developed and powerful tool, and it would be only natural to use its potential for solving the RWM tasks. Here, we essentially lean on the fundamental MHD results [3–8] and introduce new elements in the manner of extension of the classical theory.

In a general case, the force balance for the plasma is described by

$$\rho \frac{\mathrm{d}\boldsymbol{v}}{\mathrm{d}t} = -\nabla p + \boldsymbol{j} \times \boldsymbol{B} + \boldsymbol{N}, \tag{2.4}$$

where ρ is the plasma mass density, $\mathrm{d}/\mathrm{d}t = \partial/\partial t + \boldsymbol{v} \cdot \nabla$, $\boldsymbol{v}$ is the plasma velocity, t is the time, p is the plasma pressure, $\boldsymbol{j} = \nabla \times \boldsymbol{B}$ is the current density, $\boldsymbol{B}$ is the magnetic field and $\boldsymbol{N}$ is the force responsible for the non-ideal effects, plasma rotation and/or anisotropy or some external force ($\boldsymbol{N} = 0$ in the ideal MHD). Equation (2.4) is supplemented by the Maxwell equations that serve as a common basis uniting the regions with different properties (plasma, vacuum, metal). Finally, we have to add Ohm's law for the wall. This system, with proper boundary conditions, is used for deriving the energy relations in §§ 3 and 4 and, later, for calculating the RWM growth rate. Hereinafter, the units are chosen so that the magnetic pressure is $\boldsymbol{B}^2/2$ (which should be replaced by $\boldsymbol{B}^2/(2\mu_0)$ in SI units).

One possible improvement on the way to a better theory for RWMs could be the inclusion of more terms in $\boldsymbol{N}$ in (2.4). However, it cannot be an only strategy because the accuracy and adequacy of its solutions also depend on the boundary conditions. In § 5, these are discussed with examples of how they can affect the stability results. A general comparison theorem on the wall stabilization is presented in § 6.

The boundary conditions at the resistive wall depend on the perturbation penetration through the wall. Its calculation becomes an additional step if the ideal wall or magnetically-thin wall simplifications are waived, which is briefly discussed with emphasis on the case with a strong skin effect in § 7. This completes the mathematical background, and next follow the applications.

3. Energy relations in the inner region

A small displacement $\boldsymbol{\xi}$ from equilibrium is described by the equation

$$\rho_0 \frac{\partial^2 \boldsymbol{\xi}}{\partial t^2} = \boldsymbol{F}(\boldsymbol{\xi}) + \delta \boldsymbol{N}(\boldsymbol{\xi}) \tag{3.1}$$

obtained by linearizing (2.4). Here $\delta \boldsymbol{N}$ represents the input from $\boldsymbol{N} - \rho(\boldsymbol{v} \cdot \nabla)\boldsymbol{v}$,

$$\boldsymbol{F} = -\nabla \tilde{p} + \boldsymbol{j}_0 \times \boldsymbol{b} + \tilde{\boldsymbol{j}} \times \boldsymbol{B}_0 \tag{3.2}$$

is the standard MHD force operator with $\tilde{p} = p - p_0$ the pressure perturbation, $\boldsymbol{j}_0$ and $\boldsymbol{B}_0$ the equilibrium current density and magnetic field and $\tilde{\boldsymbol{j}} = \nabla \times \boldsymbol{b}$ with $\boldsymbol{b}$ a small perturbation:

$$\boldsymbol{B} = \boldsymbol{B}_0 + \boldsymbol{b}. \tag{3.3}$$

In typical cases, the solution to (3.1) can be expressed through two eigenfunctions with sin, cos or exp dependence on time and angles. Then it is convenient to introduce the complex variables as in (2.1). Representing a real perturbation $\boldsymbol{\xi}$ in such a form,

https://doi.org/10.1017/S0022377815001403 Published online by Cambridge University Press

multiplying (3.1) by $\boldsymbol{\xi}^*$ (the complex conjugate) and integrating over the plasma volume V_{pl}, one obtains

$$\delta K + W_p + N = S_p, \tag{3.4}$$

where N denotes a contribution from $\delta \boldsymbol{N}$ and other non-ideal effects such as, for example, plasma resistivity and non-adiabaticity,

$$\delta K \equiv \frac{1}{2}\int_{V_{pl}} \rho_0 \boldsymbol{\xi}^* \frac{\partial^2 \boldsymbol{\xi}}{\partial t^2}\,\mathrm{d}V, \tag{3.5}$$

$$W_p \equiv \frac{1}{2}\int_{V_{pl}} [|\boldsymbol{b}|^2 + \Gamma p_0 |\mathrm{div}\,\boldsymbol{\xi}|^2 + (\boldsymbol{\xi}\cdot\boldsymbol{\nabla} p_0)\mathrm{div}\,\boldsymbol{\xi}^* - \boldsymbol{\xi}^*\cdot(\boldsymbol{j}_0\times\boldsymbol{b})]\,\mathrm{d}V, \tag{3.6}$$

$$S_p \equiv -\frac{1}{2}\oint_{S_{pl}} (\tilde{p} + \boldsymbol{b}_i\cdot\boldsymbol{B}_{0i})\boldsymbol{\xi}^*\cdot\mathrm{d}\boldsymbol{S}, \tag{3.7}$$

Γ is the ratio of the specific heats, S_{pl} is the plasma boundary and the subscript i in (3.7) means the inner side of S_{pl}. We do not show the details of the derivations because they can be found in [3–8] and other textbooks and papers on the energy principle. In particular, at $N = 0$, (3.4) corresponds to (2) in [43] where it was further reduced in the thin-wall approximation. In the standard ideal MHD model [3–8], expressions (3.6) and (3.7) are obtained from (3.1) and (3.2) with $\boldsymbol{b} = \boldsymbol{\nabla}\times(\boldsymbol{\xi}\times\boldsymbol{B}_0)$, $\tilde{p} = -\boldsymbol{\xi}\cdot\boldsymbol{\nabla} p_0 - \gamma p_0\,\mathrm{div}\,\boldsymbol{\xi}$ and $\boldsymbol{B}_0\cdot\mathrm{d}\boldsymbol{S}_{pl} = 0$. Here, without these restrictions on $\boldsymbol{b}$ and $\tilde{p}$, the difference from the static ideal MHD is represented by N in (3.4).

In traditional stability theory [3–8], the last term on the right-hand side of (3.7) is transformed by using the force-balance equation at the plasma edge and the condition

$$\boldsymbol{n}_{pl}\times(\boldsymbol{E}_e + \boldsymbol{v}\times\boldsymbol{B}_e) = 0 \tag{3.8}$$

following from the continuity of the tangential component of $\boldsymbol{E}$ at S_{pl} (the subscript e means its external side) under the ideal-plasma constraint $\boldsymbol{E} + \boldsymbol{v}\times\boldsymbol{B} = 0$. When the equilibrium velocity $\boldsymbol{v}_0$ is small at the plasma edge, with (3.8) one obtains

$$\int_{S_{pl}} (\boldsymbol{b}_e\cdot\boldsymbol{B}_{0e})\dot{\boldsymbol{\xi}}^*\cdot\mathrm{d}\boldsymbol{S} = \int_{S_{pl}} (\boldsymbol{E}_e^*\times\boldsymbol{b}_e)\cdot\mathrm{d}\boldsymbol{S}. \tag{3.9}$$

This looks similar to the last term in (3.7), but contains $\boldsymbol{B}_0$ and $\boldsymbol{b}$ at the outer side of S_{pl} and $\dot{\boldsymbol{\xi}}^* \equiv \partial\boldsymbol{\xi}^*/\partial t$ which reduces to $\gamma^*\boldsymbol{\xi}^*$ if the time behaviour of the perturbations is described by $\exp(\gamma t)$. This is an intermediate step in the standard ideal MHD where $\boldsymbol{E}$ is eliminated at once by further transformations, see [3–8]. Here we do not follow this tradition. Keeping the term with $\boldsymbol{E}$ in this form, and allowing for other physics than that implied by (3.8) and (3.9), we can cast (3.4) in the form

$$\delta K + W_p + N + W_s = -\frac{1}{2\gamma^*}\int_{S_{pl}} (\boldsymbol{E}_e^*\times\boldsymbol{b}_e)\cdot\mathrm{d}\boldsymbol{S}, \tag{3.10}$$

where W_s is a surface integral such that $W_s + S_p$ gives the right-hand side of (3.10).

In the ideal MHD, $N = 0$ and W_s reduces to standard expressions (at $\boldsymbol{v}_0 = 0$, see the last integral in (2.7) in [4], (8.97b) in [5] or (8.47) in [6]). Here, we mention the ideal MHD as a reference model and include its results as a part of our more general approach for a potentially non-ideal plasma.

https://doi.org/10.1017/S0022377815001403 Published online by Cambridge University Press

In any case, the plasma properties are contained on the left-hand side of (3.10), while the right-hand side remains the same for any plasma model. The latter property makes (3.10) a convenient starting point for stability analysis, especially when the influence of the outer area should be investigated.

It follows from the Maxwell equations

$$\nabla \times \boldsymbol{E} = -\partial \boldsymbol{b}/\partial t, \tag{3.11}$$

$$\nabla \times \boldsymbol{b} = \tilde{\boldsymbol{j}} \tag{3.12}$$

that

$$\nabla \cdot (\boldsymbol{E}^* \times \boldsymbol{b}) = -\tilde{\boldsymbol{j}} \cdot \boldsymbol{E}^* - \gamma^* |\boldsymbol{b}|^2. \tag{3.13}$$

With its integral consequence, (3.10) is transformed into

$$\delta K + W_p + N + W_s + W_g = -F, \tag{3.14}$$

where W_g represents the magnetic energy of the perturbation in the plasma–wall vacuum gap,

$$W_g = \int_{gap} \frac{|\boldsymbol{b}|^2}{2} \, \mathrm{d}V, \tag{3.15}$$

and F describes the Poynting vector flux through the wall:

$$F \equiv \frac{1}{2\gamma^*} \int_{wall-} (\boldsymbol{E}^* \times \boldsymbol{b}) \cdot \mathrm{d}\boldsymbol{S}_w. \tag{3.16}$$

Here '*wall*−' denotes the inner surface of the vacuum chamber, S_w, to distinguish it further from the outer surface of the wall '*wall*+', $\mathrm{d}\boldsymbol{S}_w = \boldsymbol{n}_w \, \mathrm{d}S_w$ is the oriented element of the area of S_w and $\boldsymbol{n}_w$ is the outward unit normal to S_w.

4. Energy relations in the outer region

In classical stability theory [3–8], the wall is assumed ideal. This makes $F = 0$ in (3.14). Moving the wall outwards and reducing its effect on the plasma, we arrive at the 'no wall' limit with the same $F = 0$, but with integration in (3.15) extended to infinity.

The condition $F = 0$ strictly isolates the plasma from the external world. With a resistive wall, this isolation is broken. Then $F \neq 0$, which is an essentially new element compared to [3–8]. We already know that it can strongly affect the solution of (3.14) converting the ideal MHD modes in the RWMs.

The studies of RWMs are ultimately aimed at developing a strategy allowing stable operation in the region where the RWMs are potentially unstable. The experiments show that this requires either plasma rotation or feedback control or both [2, 10, 19, 20, 29]. In all cases, a reliable description of the 'open loop' system is needed as a basis for analysis. This means a correct calculation of the plasma interaction with the passive elements, which are simply called 'wall'.

The interaction explicitly enters through F, but also modifies W_g in (3.14). The flux F can be either prescribed by the boundary conditions at S_w or found from the energy balance obtained by integrating the Poynting theorem (3.13) over the space behind the toroidal surface S_w. In typical models of real tokamaks or stellarators [1, 2, 10, 12–14, 32–46, 49–79] this means integration over the wall and the external vacuum region. Then the result is

$$F = D_w + W_w + W_{w+} \tag{4.1}$$

https://doi.org/10.1017/S0022377815001403 Published online by Cambridge University Press

with D_w representing the resistive dissipation in the wall,

$$D_w \equiv \frac{1}{2\gamma^*}\int_{wall} \tilde{\boldsymbol{j}}\cdot\boldsymbol{E}^*\,\mathrm{d}V = \frac{1}{2\gamma^*}\int_{wall}\sigma|\boldsymbol{E}|^2\,\mathrm{d}V, \tag{4.2}$$

where Ohm's law in the form $\tilde{\boldsymbol{j}} = \sigma\boldsymbol{E}$ is used for the wall, and

$$W_w = \int_{wall}\frac{|\boldsymbol{b}|^2}{2}\,\mathrm{d}V, \quad W_{w+} = \int_{wall+}\frac{|\boldsymbol{b}|^2}{2}\,\mathrm{d}V, \tag{4.3a,b}$$

represent the magnetic energies in the wall and in the vacuum region behind the wall, respectively. In a more general case with some sources of $\boldsymbol{b}$ behind S_{w+} (correction coils or passive elements), a proper additional source term should be added in (4.1).

With $\boldsymbol{b} = \nabla\varphi$ in a vacuum we have

$$W_{w+} = -\frac{1}{2}\oint_{wall+}\varphi_+\boldsymbol{b}_+^*\cdot\mathrm{d}\boldsymbol{S}_w, \tag{4.4}$$

where the integration is performed over the outer side of the wall.

The flux F can be similarly expressed as

$$F = -\frac{1}{2}\oint_{wall-}\varphi_-\boldsymbol{b}_-^*\cdot\mathrm{d}\boldsymbol{S}_w, \tag{4.5}$$

but with integration over the inner side. The latter equality is obtained from (3.16) by using the identity

$$\boldsymbol{E}^*\times\boldsymbol{b} = \boldsymbol{E}^*\times\nabla\varphi = -\nabla\times(\varphi\boldsymbol{E}^*) + \varphi\nabla\times\boldsymbol{E}^*. \tag{4.6}$$

The potentials and fields are different in (4.4) and (4.5) because of the currents in the wall which also determine the magnitude of the dissipation term D_w. It follows from (4.2) that

$$D_w = \gamma\tau_w D_0, \tag{4.7}$$

with D_0 a function of $\boldsymbol{E}/\gamma$ only, and

$$\tau_w \equiv \sigma_0 r_w d_w. \tag{4.8}$$

This constant (often called the wall time [10, 21, 46]) naturally appears in the thin-wall cylindrical models with $\sigma = \sigma_0 = \text{const.}$, which will be used to derive estimates later. In such models with a uniform wall, the parameters σ_0, r_w and d_w have clear meaning, but here they should be considered as 'average' or 'fitting' values so that (4.8) does not impose any restriction on the wall.

In (4.7), D_0 is a positive real quantity proportional to the volume integral in (4.2). If $\sigma|\boldsymbol{E}|^2$ could be constant across the wall (the key assumption in the thin-wall models), D_0 would reduce to the surface integral

$$D_0^{sh} \equiv \frac{V_w}{2\tau_w}\frac{\langle\sigma|\boldsymbol{E}_-|^2\rangle}{|\gamma|^2} = \frac{S_w}{2r_w}\frac{\langle|\boldsymbol{E}_-|^2\sigma/\sigma_0\rangle}{|\gamma|^2} \tag{4.9}$$

with $V_w = S_w d_w$ the wall volume, $\boldsymbol{E}_-$ the electric field at the inner side of the wall and the brackets denoting averaging over S_w.

https://doi.org/10.1017/S0022377815001403 Published online by Cambridge University Press

This is actually an upper estimate for D_0. In fact,

$$D_0 = \alpha D_0^{sh} \tag{4.10}$$

with $\alpha \leqslant 1$ because of the radial decline of $\boldsymbol{E}$ in the wall:

$$\alpha \equiv \frac{D_w}{\gamma \tau_w D_0^{sh}} = \int_{wall} \frac{\sigma |\boldsymbol{E}|^2}{\langle \sigma |\boldsymbol{E}_-|^2 \rangle} \frac{\mathrm{d}V}{V_w}. \tag{4.11}$$

To express D_0^{sh} and α in terms of the magnetic quantities, like those in (4.4) and (4.5), we have to solve (3.11). The task is simplified if the wall is geometrically thin. Then with $\tilde{\boldsymbol{j}} = \sigma \boldsymbol{E}$ we need only the tangential component of $\boldsymbol{E}$ described by

$$|\nabla a| \frac{\partial}{\partial t} \boldsymbol{b} \cdot \boldsymbol{n} = \nabla \cdot (\nabla a \times \boldsymbol{E}), \tag{4.12}$$

which is a consequence of (3.11). Here $a(\boldsymbol{r}) = \text{const.}$ is some parameterization of the family of the nested toroidal surfaces with $a = a_w$ and $a = a_w + d_w |\nabla a|$ representing the inner and outer sides of the wall (S_w and S_{w+}), respectively. The operator on the right-hand side of (4.12) is two-dimensional and can be easily inverted, providing us with $\boldsymbol{E}$ and D_0 as functions of $\boldsymbol{b} \cdot \boldsymbol{n}$.

The remaining quantity in (4.1), W_w, is small compared to W_{w+} if the wall is thin and penetration of $\boldsymbol{b}$ through the wall is good. These two conditions (with $\boldsymbol{b} \cdot \boldsymbol{n}$ the same at the inner and outer sides of the wall) constitute the basis of the thin-wall models [2, 10, 13, 14, 16, 25, 35, 41–43, 46, 49, 53–64, 68, 73, 76–79]. Then

$$W_w = \int_{wall} \frac{|\boldsymbol{b}|^2}{2} \mathrm{d}V < \frac{\max |\boldsymbol{b}|^2}{2} V_w, \tag{4.13}$$

and $W_w / W_{w+} \sim d_w / r_w \ll 1$ for the kink-like perturbations such as in (2.3).

Disregard of W_w in favour of W_{w+} is considered natural in the thin-wall models [10, 35, 43, 46]. However, it can be justified at $s \gg d_w$ only. Outside this rather narrow range, the skin effect inhibits the amplitude of $\boldsymbol{b}$ in the wall, so that finally we can expect the opposite $W_w / W_{w+} \gg 1$ at $0 < s \ll d_w$ [80, 81]. Below, both cases will be considered.

5. Boundary conditions

Two equations, (3.14) and (4.1), represent two parts of the system divided by S_w. These equations could be used separately if the boundary conditions were properly prescribed at S_w.

These conditions, needed to calculate W_g and F in (3.14), essentially affect the results of the stability analysis. This can be illustrated by the difference between β_N^{wall} and $\beta_N^{no\,wall}$, the stability limits for the same configuration computed, respectively, with ideal wall and without wall, in terms of the frequently used parameter

$$\beta_N = \beta\ (\%) \frac{a\ (\mathrm{m})\ B\ (\mathrm{T})}{I\ (\mathrm{MA})}, \tag{5.1}$$

where a is the minor radius of the plasma, B is the magnetic field and I is the net current in the plasma. The representative examples are $\beta_N^{wall} = 3.5$–4 and $\beta_N^{no\,wall} = 2$–2.5 in ITER [2], $\beta_N^{wall} = 3.3$ and $\beta_N^{no\,wall} = 1.8$–2.2 in the DIII-D tokamak [12], $\beta_N^{wall} = 4.3$ and $\beta_N^{no\,wall} = 2$ in JT-60SA [26] and $\beta_N^{wall} = 5$ with $\beta_N^{no\,wall} = 2.5$ in KSTAR [82]. For more data and details see table II in [21], figures 3 and 4 in [83] and discussion in [65].

https://doi.org/10.1017/S0022377815001403 Published online by Cambridge University Press

The ideal-wall models require $\boldsymbol{b}\cdot\boldsymbol{n}_w = 0$. In the stability theory, this was usually introduced as $\boldsymbol{n}_w \times \boldsymbol{E} = 0$ without alternatives [3, 4, 6–8], though in [5] it was noted that, in some cases, the wall resistivity should be taken into account.

An ideal wall means no penetration of the perturbation through S_w. If, on the contrary, the penetration is perfect, so that $\boldsymbol{b}\cdot\boldsymbol{n}_w \neq 0$ is the same at the both sides of the wall, we have the so-called thin-wall approximation, the dominant approach in the existing RWM theory. In practice, the walls are geometrically thin (with a thickness d_w much smaller than the minor radius r_w), but for constant $\boldsymbol{b}\cdot\boldsymbol{n}_w$ across the wall we need $s/d_w \gg 1$, where s is the skin depth. This allows slow modes only. The ideal-wall assumption corresponds to the opposite limit $s/d_w \to 0$. The intermediate range around $s/d_w = 1$ remains basically unexplored, which prompts us to fill this gap in theory.

In a general case, the normal component of $\boldsymbol{b}$ is not zero at S_w and varies with distance across the wall so that $\boldsymbol{b}\cdot\boldsymbol{n}_w$ is different at S_w and S_{w+}. Then a self-consistent prescription of $\boldsymbol{b}$ at the inner side of the wall depends on the $\boldsymbol{b}(\boldsymbol{r})$ behaviour in and behind the wall through the natural boundary conditions

$$[[\boldsymbol{n}\cdot\boldsymbol{b}]] = 0, \quad [[\boldsymbol{n}\times\boldsymbol{b}/\mu]] = 0 \tag{5.2a,b}$$

at the wall–vacuum interfaces. Here the brackets $[[\cdots]]$ mean the jump across the surface and μ is the magnetic permeability. In the RWM theory, usually ferromagnetic effects are disregarded, which is justified by analytical and numerical analysis [84, 85] for slow modes. The situation is different for fast modes (at $s < d_w$) [86], which can be expected in future experiments in the JT-60SA tokamak [26] and, possibly, in experiments with a movable ferromagnetic wall in the HBT-EP tokamak [87]. However, more often the results obtained with $\mu = 1$ are good enough and can be easily extended to the area with $\mu \neq 1$ [86]. This is why $\mu = 1$ is assumed in what follows.

With (5.2), calculation of $\boldsymbol{b}(\boldsymbol{r})$ in the wall becomes a part of the problem. In the earlier plasma stability theory, this task was avoided by assuming the wall to be ideal. Later, it was addressed in the most simple thin-wall formulation. These approaches are well developed, so more attention will be focused here on the intermediate case with a magnetically thick resistive wall.

6. Wall stabilization in terms of W_g

The benefits of the ideal wall stabilization in several tokamaks are explicitly demonstrated in the previous section. In reality, the walls are not perfect conductors and can produce only a partial stabilizing effect compared to the ideal case. Even this seems attractive for the success of a steady-state tokamak reactor [1]. Being an issue of particular importance for ITER, it was discussed in detail in [1, 2]. A nice review of the problem was recently given in [10]. Here we mostly concentrate on the relevant theoretical aspects with more emphasis on yet unexplored areas.

When (3.14) is applied to the system with an ideal wall, it reduces to

$$\gamma^2 K_0 = -(W_p + N + W_s) - W_g \tag{6.1}$$

with

$$K_0 \equiv \frac{1}{2}\int_{V_{pl}} \rho_0 |\boldsymbol{\xi}|^2 \, \mathrm{d}V. \tag{6.2}$$

https://doi.org/10.1017/S0022377815001403 Published online by Cambridge University Press

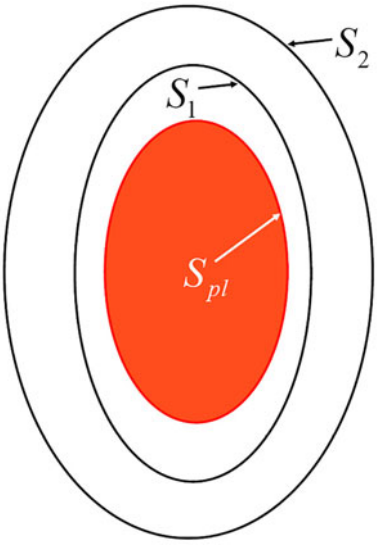


FIGURE 4. Schematic view of two configurations with the same plasma and different walls. S_{pl} is the plasma surface, S_1 is the wall in the case 1, and S_2 is the wall in the case 2.

In the static ideal MHD, (6.1) is further simplified, its right-hand side becomes real [3–8] with quantities containing γ only through $\exp(\gamma t)$ dependence of $\boldsymbol{\xi}$ and $\boldsymbol{b}$. It is clear that both K_0 and W_g are positive, which means that the term W_g is always stabilizing. At given plasma parameters, its contribution to (6.1) depends on the wall shape and location.

Precise evaluation of W_g requires a knowledge of $\boldsymbol{b}(\boldsymbol{r})$ in the plasma–wall gap, but useful comparisons can be made in a general form using the property that $\boldsymbol{b}(\boldsymbol{r})$ in this vacuum region is determined by the normal component of $\boldsymbol{b}$ at the boundary. This includes the wall, where $\boldsymbol{b}\cdot\boldsymbol{n}_w = 0$ if it acts as an ideal conductor, and the plasma boundary S_{pl}.

Consider two cases with the same plasma and the same $\boldsymbol{b}\cdot\boldsymbol{n}_{pl}$ at S_{pl}, but with different ideal walls, as schematically shown in figure 4. Then we have two toroidal vacuum regions, 1 (smaller) bounded by S_1 and 2 (larger) bounded by S_2 with common interior boundary S_{pl}. In these regions, the magnetic perturbations $\boldsymbol{b}_1 = \nabla\varphi_1$, representing case 1, and $\boldsymbol{b}_2 = \nabla\varphi_2$ in the case 2 must satisfy the same boundary conditions $\boldsymbol{b}_1\cdot\boldsymbol{n}_{pl} = \boldsymbol{b}_2\cdot\boldsymbol{n}_{pl}$ at S_{pl} and $\boldsymbol{b}_1\cdot\boldsymbol{n}_{w1} = 0$ and $\boldsymbol{b}_2\cdot\boldsymbol{n}_{w2} = 0$ at the corresponding outer boundaries S_1 and S_2.

Since $\boldsymbol{b}_1 = 0$ between S_1 and S_2 and, naturally, $\operatorname{div}\boldsymbol{b}_1 = \operatorname{div}\boldsymbol{b}_2 = 0$, we have

$$\int_2 \boldsymbol{b}_1\cdot\boldsymbol{b}_2\,\mathrm{d}V = \int_1 \boldsymbol{b}_1\cdot\boldsymbol{b}_2\,\mathrm{d}V = \int_1 \operatorname{div}(\varphi_2\boldsymbol{b}_1)\,\mathrm{d}V = \int_{S_1} \varphi_2\boldsymbol{b}_1\cdot\mathrm{d}\boldsymbol{S} - \int_{S_{pl}} \varphi_2\boldsymbol{b}_1\cdot\mathrm{d}\boldsymbol{S}. \quad (6.3)$$

Both walls are assumed ideal, which makes the integral over S_1 zero. Then replacing $\boldsymbol{b}_1\cdot\mathrm{d}\boldsymbol{S}_{pl}$ by $\boldsymbol{b}_2\cdot\mathrm{d}\boldsymbol{S}_{pl}$ in the integral over S_{pl}, we can transform (6.3) into

$$\int_2 \boldsymbol{b}_1\cdot\boldsymbol{b}_2\,\mathrm{d}V = -\int_{S_{pl}} \varphi_2\boldsymbol{b}_2\cdot\mathrm{d}\boldsymbol{S} = \int_2 \operatorname{div}(\varphi_2\boldsymbol{b}_2)\,\mathrm{d}V - \int_{S_2} \varphi_2\boldsymbol{b}_2\cdot\mathrm{d}\boldsymbol{S}_2. \quad (6.4)$$

https://doi.org/10.1017/S0022377815001403 Published online by Cambridge University Press

With $\boldsymbol{b}_2 \cdot \mathrm{d}\boldsymbol{S}_2 = 0$ the last term vanishes so that

$$\int_2 \boldsymbol{b}_1 \cdot \boldsymbol{b}_2 \,\mathrm{d}V = \int_2 \mathrm{div}(\varphi_2 \boldsymbol{b}_2)\,\mathrm{d}V = \int_2 \boldsymbol{b}_2^2 \,\mathrm{d}V. \tag{6.5}$$

Using this equality and the identity

$$\int (\boldsymbol{b}_2 - \boldsymbol{b}_1)^2 \,\mathrm{d}V = \int \boldsymbol{b}_2^2 \,\mathrm{d}V + \int \boldsymbol{b}_1^2 \,\mathrm{d}V - 2\int \boldsymbol{b}_1 \cdot \boldsymbol{b}_2 \,\mathrm{d}V \tag{6.6}$$

valid for any volume, we obtain finally

$$\int_1 \boldsymbol{b}_1^2 \,\mathrm{d}V = \int_2 \boldsymbol{b}_2^2 \,\mathrm{d}V + \int_2 (\boldsymbol{b}_2 - \boldsymbol{b}_1)^2 \,\mathrm{d}V. \tag{6.7}$$

The latter means that, in two similar configurations with different ideal walls, the magnetic energy W_g must be larger when the wall is closer to the plasma. Using figure 4 as an example, we can say that (6.7) proves that the wall S_1 provides stronger stabilization than the wall S_2. This is a general rule for any perturbation.

7. Perturbations in the wall

In the geometrically thin walls, the current density can be approximated by

$$\boldsymbol{j} = \boldsymbol{\nabla}\kappa \times \boldsymbol{\nabla} a, \tag{7.1}$$

which corresponds to

$$\boldsymbol{b} = \kappa \boldsymbol{\nabla} a + \boldsymbol{\nabla}\varphi \tag{7.2}$$

with

$$\nabla^2 \varphi = -\mathrm{div}(\kappa \boldsymbol{\nabla} a) \tag{7.3}$$

because of $\mathrm{div}\,\boldsymbol{b} = 0$ (outside the wall, $\kappa = 0$). Here a is the same 'radial' coordinate as introduced in (4.12).

For an axially symmetric toroidal wall with $\sigma = \mathrm{const.}$ and perturbations depending on the toroidal angle ζ as $\exp(in\zeta)$, one obtains from the projection of (3.11) on $\boldsymbol{\nabla}\zeta$:

$$\sigma \frac{\partial \varphi}{\partial t} = -R^2\,\mathrm{div}\frac{\kappa \boldsymbol{\nabla} a}{R^2} \approx -\mathrm{div}(\kappa \boldsymbol{\nabla} a), \tag{7.4}$$

where $|\boldsymbol{\nabla}\zeta| = 1/R$, R is the radius counted from the main axis, and the approximate equality corresponds to disregard of the toroidal corrections. Two last equations yield

$$S^2 \nabla^2 \varphi = \varphi, \tag{7.5}$$

where S is a complex quantity defined by

$$1/S^2 \equiv \sigma\gamma. \tag{7.6}$$

In a general case, in the resistive wall with $\sigma = \mathrm{const.}$ and $\mu = 1$, the perturbation is governed by the equation

$$\sigma \frac{\partial \boldsymbol{b}}{\partial t} = \nabla^2 \boldsymbol{b}. \tag{7.7}$$

In a cylinder, its z-component gives the same equation for b_z as (7.5) for φ.

https://doi.org/10.1017/S0022377815001403 Published online by Cambridge University Press

The ideal wall and conventional thin-wall approximations are the most simple idealizations. A natural question is what can be gained from more realistic description of the wall? The answer is that, in addition to increasing accuracy in calculations of the growth rates [80, 81, 88, 89], new effects may appear [65–67] that are not predicted in the mentioned ideal- and thin-wall limits. The most interesting must be the region between these extremes, where the wall may look almost ideal in suppressing $\boldsymbol{b}\cdot\boldsymbol{n}_w$, but still provides an energy sink. With a resistive wall, a combination of these properties is achieved due to the skin effect completely ignored in conventional stability theory.

Assuming a strong skin effect, so that ∇^2 can be replaced by $\partial^2/\partial\ell^2$ with ℓ the distance from S_w along the normal, we can approximate the solution of (7.5) and the radial dependence of $\boldsymbol{b}$ in the wall by $\exp(-\ell/S)$. Accordingly, $\tilde{\boldsymbol{j}}=\nabla\times\boldsymbol{b}\approx(\boldsymbol{b}\times\boldsymbol{n}_w)/S$ and

$$\sigma S\boldsymbol{E}\approx\boldsymbol{b}\times\boldsymbol{n}_w, \tag{7.8}$$

where Ohm's law has been used.

In addition to (7.8), we also need $\boldsymbol{b}\cdot\boldsymbol{n}_w$ for calculation of W_w in (4.3). For the fast modes with low and intermediate m (poloidal wavenumber) and $s\ll d_w$, this component must be small:

$$\frac{|\boldsymbol{b}\cdot\boldsymbol{n}_w|}{|\boldsymbol{b}\times\boldsymbol{n}_w|}\sim\frac{ms}{r_w}=\frac{md_w}{r_w}\frac{s}{d_w}\ll 1, \tag{7.9}$$

which follows from $\operatorname{div}\boldsymbol{b}=0$. When this is satisfied, with (7.8), we obtain

$$W_w\approx\int_{wall}\frac{|\boldsymbol{b}\times\boldsymbol{n}_w|^2}{2}\,\mathrm{d}V\approx\frac{\gamma^*}{|\gamma|}D_w \tag{7.10}$$

with D_w defined by (4.2).

Note that in this limit (at $s\ll d_w$) the perturbation practically does not penetrate through the wall, which makes $W_{w+}\ll W_w$.

With only this fact, we can conclude that the skin effect must change the stability predictions because in the marginal thin-wall limit (at $s\gg d_w$) the magnetic energy inside the wall with $d_w\ll r_w$ is negligible compared to W_{w+}. This is simply because the wall volume is small and the magnetic perturbation in and just behind the wall must be of the same order, if $\boldsymbol{b}\cdot\boldsymbol{n}_w$ is assumed constant across the wall. For more details see cylindrical estimates in [67, 90].

Equation (7.9) shows that the normal component of $\boldsymbol{b}$ decreases with decreasing s. It goes to zero at $s\to 0$, which corresponds to the transition to the ideal-wall limit. In the latter case, $D_w=0$ and (4.1) turns into $F=0$. Our main interest is the range with small but finite s/d_w when the wall looks 'almost ideal' strongly suppressing $\boldsymbol{b}\cdot\boldsymbol{n}_w$, but the energy dissipation in the wall still plays a role in the total energy balance.

8. Thin-wall and thick-wall dispersion relations

Equation (4.1) gives us

$$\gamma\tau_w=\frac{F-W_w-W_{w+}}{D_0} \tag{8.1}$$

with D_0 introduced by (4.7). This equation can be applied to toroidal systems in combination with (3.14) relating F to the plasma parameters. Equation (8.1) is

https://doi.org/10.1017/S0022377815001403 Published online by Cambridge University Press

meaningful provided that $D_0 \neq 0$, which is satisfied when the perturbation penetrates into the wall. Otherwise, (4.1) turns into $0 = 0$ and only (3.14) with $F = 0$ remains without any effect of the wall resistivity.

In (8.1), only F explicitly depends on the plasma through (3.14). The reaction on F of all other quantities on the right-hand side depends on the radial behaviour of $\boldsymbol{b}$ in the wall. Next we consider a geometrically thin wall with $d_w \ll r_w$ and compare two cases, one with $s \gg d_w$ (traditional slow RWMs) and another with $s \ll d_w$ (fast RWMs).

When $s \gg d_w$, both $\tilde{\boldsymbol{j}}$ and $\boldsymbol{E}$ are almost constant across the wall, and (4.10) and (4.11) give $\alpha = 1$ and $D_0 = D_0^{sh}$ independent of γ. Then (8.1) is a resolved dispersion relation.

At the opposite $s \ll d_w$, the radial variation of $\tilde{\boldsymbol{j}}$ and $\boldsymbol{E}$ inside the wall is large. It can be approximately described by $|\boldsymbol{E}| = |\boldsymbol{E}_-| \mathrm{e}^{-\ell/s}$, where

$$\frac{1}{s} = \mathrm{Re}\frac{1}{S} = \mathrm{Re}\sqrt{\sigma\gamma} \tag{8.2}$$

and S is defined by (7.6). With such $\boldsymbol{E}$, (4.11) yields

$$\alpha = \frac{s}{2d_w}, \tag{8.3}$$

which is small for the case considered and decreases with increasing $|\gamma|$. Then $D_0 = \alpha(\gamma) D_0^{sh}$ that makes (8.1) an unresolved equation for γ.

It follows from (4.7) and (7.10) that, for the fast RWMs, $W_w/D_0 = |\gamma|\tau_w$. With this relation and (4.10) with α given by (8.3) we obtain from (8.1)

$$\gamma + |\gamma| = \frac{2d_w}{s}\gamma^{sh}, \tag{8.4}$$

where γ^{sh} is defined by

$$\gamma^{sh}\tau_w \equiv \frac{F - W_{w+}}{D_0^{sh}}. \tag{8.5}$$

Equation (8.4) can serve as a dispersion relation at $s \ll d_w$. For consistency, we should skip W_{w+} in (8.5) because $W_{w+} \ll W_w$ in this case. With W_{w+} retained and the opposite ordering $W_{w+} \gg W_w$, (8.5) gives us the growth rate in the thin-wall approximation which can be used at $s \gg d_w$ only.

With (8.2) we obtain from (8.4)

$$\gamma\tau_{sk} = (\gamma^{sh}\tau_{sk})^2, \tag{8.6}$$

where γ is the true growth rate at $s \ll d_w$, γ^{sh} is the thin-wall estimate (though far behind the applicability region of the thin-wall approximation), and

$$\tau_{sk} \equiv \sigma d_w^2 = \tau_w d_w / r_w. \tag{8.7}$$

Finally, we have two distinctly different dispersion relations for the modes interacting with a resistive wall. One is obtained in the standard thin-wall model, which assumes $\boldsymbol{b} \cdot \boldsymbol{n}_w$ identical on the both sides of the wall:

$$\gamma^{sh}\tau_{sk} = g_m. \tag{8.8}$$

https://doi.org/10.1017/S0022377815001403 Published online by Cambridge University Press

Another is obtained assuming the same wall to be magnetically thick so that $\boldsymbol{b}\cdot\boldsymbol{n}_w = 0$ behind the wall:

$$\gamma\tau_{sk} = g_m^2. \tag{8.9}$$

In these relations,

$$g_m \equiv \frac{d_w}{r_w}\frac{F - W_{w+}}{D_0^{sh}}, \tag{8.10}$$

where W_{w+} can be disregarded when applied to the fast modes. Then g_m is determined by two surface integrals over the inner side of the wall. By definition, D_0^{sh} is a real quantity. The imaginary part of g_m can appear from F only. Note that (8.8) and (8.9), one valid for slow modes with $s \gg d_w$ and the other for fast modes with $s \ll d_w$, have been obtained without restrictions on the plasma models. These relations are derived from (3.13) and (4.1) describing the energy balance outside the plasma, which is a perfect foundation free from uncertainties related to incomplete knowledge of the plasma equilibrium parameters and the perturbation dynamics.

To be precise, (3.14) and (4.1), with complex F, should be called energy–torque relations. The toroidal electromagnetic torque exerted on the plasma is

$$T \equiv \int_{V_{pl}} R\boldsymbol{e}_\zeta \cdot (\boldsymbol{j}\times\boldsymbol{B})\,\mathrm{d}V = \int_{S_{as}} RB_\zeta \boldsymbol{B}\cdot\mathrm{d}\boldsymbol{S}, \tag{8.11}$$

where S_{as} is any axisymmetric surface in the vacuum gap [91, 92]. For a magnetic perturbation with a single toroidal harmonic, we obtain in terms of the complex functions used in (4.5):

$$T = \frac{\mathrm{i}n}{4}\oint_{wall-} (\varphi_- \boldsymbol{b}_-^* - \varphi_-^* \boldsymbol{b}_-)\cdot\mathrm{d}\boldsymbol{S}_w = n\,\mathrm{Im}\,F, \tag{8.12}$$

Similarly, for $n \neq 0$ and axisymmetric S_w, $\mathrm{Re}(\gamma^* F)$ will be the Poynting vector flux through the wall.

9. Cylindrical estimates

Equation (8.1) and its reduced versions, (8.8) and (8.9), are valid for toroidal systems without limitations on the plasma shape. For a cylindrical configuration shown in figure 3, each term in (8.1) can be expressed in a form allowing easy estimates and comparisons.

In this geometry, with perturbations prescribed in the form (2.3) the surface integrals turn into

$$\oint_{wall} XY^*\,\mathrm{d}S_w = X_m Y_m^* S_w, \tag{9.1}$$

where S_w is the full area of the wall surface. When X and Y are represented by several harmonics, the right-hand side will be a sum over m. This can be applied to (4.4) and (4.5).

Another simplification comes from the use of the explicit cylindrical solutions to (7.7) in the wall and to the Laplace equation $\nabla^2\varphi = 0$ for the magnetic potential φ in vacuum. For example, in the plasma–wall vacuum gap and behind the wall, such solution for the (m, n) harmonic is

$$\varphi_m = \frac{R_0}{n}\left\{B_m^{in}\frac{\mathrm{K}_m(u)}{\mathrm{K}_m'(u_w)} + B_m^{out}\frac{\mathrm{I}_m(u)}{\mathrm{I}_m'(u_w)}\right\}. \tag{9.2}$$

https://doi.org/10.1017/S0022377815001403 Published online by Cambridge University Press

Here I_m and K_m are the modified Bessel functions, the prime denotes the derivative with respect to $u = nr/R_0$, with $2\pi R_0$ being the length of the system and $u_w = nr_w/R_0$. The complex constants B_m^{in} and B_m^{out} must be different at the opposite sides of the wall.

The radial component of $\boldsymbol{b} = \nabla\varphi$ is then given by

$$b_r = b_m(r, t) \exp \mathrm{i}(m\theta - n\zeta) \tag{9.3}$$

with

$$b_m = b_m^{in} + b_m^{out}, \tag{9.4}$$

where the first term is the part of b_m due to the currents in the inner area with respect to the point r, and the second one describes the contribution from the outer sources. These functions correspond to the two terms in (9.2). For perturbations with small m and n, one can use the approximate expressions (valid for $nr \ll mR_0$)

$$b_m^{in} = B_m^{in} x^{-m-1}, \tag{9.5}$$

$$b_m^{out} = B_m^{out} x^{m-1}, \tag{9.6}$$

where $x = r/r_w$, while B_m^{in} and B_m^{out} introduced in (9.2) are the amplitudes of b_m^{in} and b_m^{out} at $x = 1$. Then (9.2) reduces to

$$\varphi_m = \frac{r}{m}(b_m^{out} - b_m^{in}) = \frac{r}{m}(2b_m^{out} - b_m). \tag{9.7}$$

With this approximate relation for a single mode (m, n), we obtain from (4.4) and (4.5)

$$W_{w+} = \frac{r_w}{2m}\beta_m\beta_m^* S_w \tag{9.8}$$

and

$$F = \frac{r_w}{2m}(B_m - 2B_m^{out})B_m^* S_w, \tag{9.9}$$

where β_m and B_m are, respectively, the amplitudes of b_m at the outer and inner sides of the wall. Accordingly, for the considered simple case without sources of $\boldsymbol{b}$ behind the wall, B_m^{out} in (9.9) means the field produced by the wall currents. The wall is treated as geometrically thin ($d_w \ll r_w$), that is why the both equalities contain r_w. For the magnetically thin wall we could put β_m and B_m equal. In the general case, they are different. This is the reason why, finally, (8.9) differs from (8.8).

For the quantity W_w in (8.1) we can use the approximate relation $W_w = 0$ in the thin-wall limit ($s \gg d_w$) and (7.10) in the thick-wall limit ($s \ll d_w$).

To express D_0^{sh} similar to (9.8) and (9.9), we have to solve (4.12) for $\boldsymbol{E}$. If the wall is geometrically thin, E_r must be small and $\nabla \cdot \boldsymbol{E} = 0$ is approximated by

$$mR_0E_\theta = nrE_z \tag{9.10}$$

for the (m, n) harmonic described by (9.3). Then $\nabla r \times \boldsymbol{E} \approx -E_z\boldsymbol{e}_\theta$, where the term of the order of $nr/(mR_0)$ is disregarded, and (4.12) yields

$$E_z = \mathrm{i}\gamma\frac{r}{m}b_r. \tag{9.11}$$

For perturbations with $nr \ll mR_0$ we can retain E_z only in (4.9). It gives then with (9.1) and $\sigma = \sigma_0$:

$$D_0^{sh} = \frac{r_w}{2m^2}B_m B_m^* S_w. \tag{9.12}$$

https://doi.org/10.1017/S0022377815001403 Published online by Cambridge University Press

With these relations, (8.10) becomes

$$g_m = \frac{m d_w}{r_w}\left[\left(1 - \frac{\beta_m \beta_m^*}{B_m B_m^*}\right) - 2\frac{B_m^{out}}{B_m}\right], \tag{9.13}$$

where the term in the round brackets must be zero in the thin-wall case ($\beta_m = B_m$). In the thick-wall limit ($|\beta_m| \ll |B_m|$), it can be disregarded as a small correction.

The latter can be easily explained. It follows from (8.2) in combination with (8.8) and (8.9) that

$$\frac{d_w}{s} = \mathrm{Re}\begin{cases}\sqrt{g_m} & \text{at } d_w \ll s \\ g_m, & \text{at } d_w \gg s.\end{cases} \tag{9.14}$$

This shows that $|g_m|$ must be large in the thick-wall limit. To make consistent (9.13) and (9.14) at $d_w \gg s$, we need $2|B_m^{out}/B_m| \gg r_w/(m d_w)$. Then, with typical $r_w \gg d_w$ and moderate m, this will be the dominant contribution in (9.13).

The above means that in both cases, in the thin- ($s \gg d_w$) and thick-wall ($s \ll d_w$) limits, we can use the relation

$$g_m = \frac{d_w}{r_w}\Gamma_m, \tag{9.15}$$

where

$$\Gamma_m \equiv -2m\frac{B_m^{out}}{B_m} = -\frac{2m}{1 - x^{2m} + x^{2m} b_m / b_m^{out}}. \tag{9.16}$$

The latter equality is obtained with the use of (9.4)–(9.6). It gives Γ_m as a function of b_m/b_m^{out} at any point in the plasma–wall vacuum gap. In experiments, b_m can be measured by the magnetic probes. Extracting b_m^{out} from b_m requires some additional measurements and processing of data [93, 94], but finally Γ_m can be found without precise knowledge of the plasma parameters. This gives g_m, and we can use (8.8) and (8.9) either for evaluation of γ_R and ω or for comparison of the measured γ_R and ω with the model predictions.

Moving into the range of smaller $s/d_w \ll 1$, we will eventually approach the ideal-wall limit at $s = 0$. In classical stability theory [3–8], it is introduced by $\boldsymbol{n}_w \times \boldsymbol{E} = \boldsymbol{n}_w \cdot \boldsymbol{b} = 0$ at the wall. In the cylindrical model, this reduces to $B_m = 0$. Then the presented expressions in terms of B_m give us infinite g_m and $\gamma\tau_{sk}$. The latter contains τ_{sk} which is also infinite for an ideal wall. Therefore, finding the ideal-wall γ requires more careful actions than a simple substitution of $s = 0$ into the otherwise reliable and informative formulas for the fast RWMs. The transition to ideal MHD modes for large g_m and $\gamma\tau_{sk}$ is discussed in § 17.

10. Relation to other RWM models

We introduced Γ_m in (9.15) to make easier comparisons between the existing models. This is exactly the same as Γ_m in the equation

$$\tau_w \frac{\partial B_m}{\partial t} = \Gamma_m B_m - \Gamma_m^0 B_m^{ext}, \tag{10.1}$$

which has been used in the thin-wall analysis of RWMs and related effects in [77, 84, 85, 90, 93, 95]. Here $\Gamma_m^0 = -2m$ for $m \neq 0$ or $\Gamma_m^0 = -2$ for $m = 0$ and B_m^{ext} is the contribution to B_m due to sources behind the wall. For example, B_m^{ext} may be

https://doi.org/10.1017/S0022377815001403 Published online by Cambridge University Press

the error field and/or the field of the correction or feedback coils. Equation (10.1) is an integral cylindrical consequence of (7.7). At constant or zero B_m^{ext} it gives the dispersion relation

$$\gamma\tau_w = \Gamma_m, \tag{10.2}$$

which is equivalent to (8.8) combined with (8.7) and (9.15) or to (3.10) in [17].

Equations similar to (10.1) can be found in [2, 10, 13, 14, 38, 39, 43, 73]. The lumped-parameter model [12, 17] operates with a system of several equations which also reduces to (10.1).

Equation (9.16) gives a simple connection to any RWM model, including those that prescribe the plasma dynamics and present Γ_m as a function of plasma parameters. Only b_m/b_m^{out} is needed to find Γ_m and make a step towards (8.8) and (8.9). Such a procedure has been employed in [96], where the Boozer model [97, 98] was analysed to find its hidden implications and make possible their comparison with experimental results.

Instead of b_m/b_m^{out}, one can use the ratio rb_m'/b_m. This follows from [77, 90, 96]

$$\frac{rb_m'}{b_m} = -(m+1) - \frac{2m\Gamma_m x^{2m}}{2m + \Gamma_m(1-x^{2m})} \tag{10.3}$$

for the plasma–wall vacuum gap, which comes from (9.4) and (9.16) with approximate (9.5) and (9.6) that give

$$2mb_m^{out} = rb_m' + (m+1)b_m. \tag{10.4}$$

Here the prime means the radial derivative, and $x = r/r_w$.

In the Fitzpatrick–Aydemir model [99], the thin-wall dispersion relations are expressed through rb_m'/b_m at the plasma surface S_{pl}. With (10.3) they can be cast in the form of (10.2), which facilitated the detailed analysis of their consequences and comparison to the Boozer model in [100]. The boundary conditions in terms of rb_m'/b_m at the plasma edge were also prescribed in the models in [32, 36].

Equations (9.16) and (10.3) show that the plasma properties enter the task through either b_m/b_m^{out} or rb_m'/b_m at S_{pl}. These quantities may be complex making thereby

$$\Gamma_m = \tau_w(\gamma_0 + in\Omega_0), \tag{10.5}$$

where, according to (10.1), real γ_0 and Ω_0 are the natural instantaneous decay/growth rate of the mode and the angular frequency of its toroidal rotation (in the thin-wall approximation under fixed B_m^{ext} or $B_m^{ext} = 0$). In the ideal MHD, γ^2 must be real, in which case only one of these parameters survives in (10.5). This may hold true even if the resistive wall is present, though only in the thin-wall approximation [10, 35, 43, 44, 46]. Then the plasma interaction with the resistive wall is described by a single number.

Such simplification is not an attribute of some cylindrical models only. In the thin-wall code VALEN, the perturbation produced by the plasma is also modelled as a single mode described by a real Γ_m [41, 45, 82].

The approach starting from (4.1), with a detailed description of the outer region and leading to (8.1), (8.8) and (8.9) allows a unified treatment with different plasma models (ideal or non-ideal) as replaceable parts in the full task. Equations (9.16) and (10.3) also show a straightforward path for extension of the previous studies from slow to fast RWMs since both (8.8) and (8.9) contain the same g_m or, finally, Γ_m.

https://doi.org/10.1017/S0022377815001403 Published online by Cambridge University Press

11. Plasma response

To make definite conclusions from the derived dispersion relations (8.8) and (8.9), we have to know the properties of g_m. This quantity was defined by (8.10) through the integrals quadratic in $\boldsymbol{b}$ and $\boldsymbol{E}$. Equations (9.15) and (9.16) show that, in the cylindrical limit, g_m is proportional to the ratio B_m^{out}/B_m, where

$$B_m = B_m^{out} + B_m^{pl} \tag{11.1}$$

and B_m^{pl} is the contribution to B_m from the plasma. Therefore, g_m is determined by the plasma response to the perturbation from outside, B_m^{out}.

The fusion plasma too easily responds to perturbations that cannot be eliminated in advance, or properly counteracted. At the same time, to reach the goals of ITER, JT-60SA and similar projects, we need high accuracy in the predictions of these responses.

The general problem of the plasma response was recently discussed in [101–104]. In [101], the linear plasma response to resonant magnetic perturbation (RMP) and non-resonant perturbation fields was computed using the MHD code MARS-F. The response of resonant harmonics was found to be sensitive to the plasma resistivity and the toroidal rotation, while that of non-resonant harmonics was mostly sensitive to the equilibrium plasma pressure. This was a systematic study with various plasma parameters and coil configurations which led the authors to the conclusion that it is still questionable to apply these results directly to the edge localized modes (ELMs) mitigation experiments due to limitations of the model. In [103], the evidence from DIII-D experiments was presented indicating that several effects are important in the overall plasma response, so that even the vacuum model, the simplest description of the tokamak plasma response to 3-D fields, is predicted to be quite complex. In [102], an overall conclusion was that none of the analysed linear and nonlinear models are fully satisfactory. In [104], a significant disagreement has been seen between solutions of the VMEC stellarator equilibrium code and solutions of tokamak perturbative 3-D equilibrium codes.

A positive allusion in this and similar critical statements is that diagnostic capabilities and resolution have reached a level of high art. However, even with the best local measurements in the plasma, one cannot expect from theory a comprehensive picture for a very simple reason: there are too many unknowns in the problem. To solve the Maxwell equations, one needs complete knowledge of the current density distribution $\boldsymbol{j}(\boldsymbol{r})$ and the boundary conditions. The fact that the magnetic field $\boldsymbol{B}(\boldsymbol{r})$ is the integral function of all currents in the plasma means that the local plasma response will always be calculated with some error. On the other hand, the same integral nature of $\boldsymbol{B}(\boldsymbol{r})$ makes these predictions quite reliable 'in an average sense'. That is why even the cylindrical model gives useful insight into the physics of kink-like instabilities.

In the model discussed in the two previous sections,

$$B_m^{out} = B_m^{w} + B_m^{er} + B_m^{f}, \tag{11.2}$$

which includes several inputs: from the wall, B_m^w, from some unaccounted sources (error field), B_m^{er} and from the correction coils, B_m^f. The latter can be used as a known perturbation to find Γ_m or g_m by the measured plasma reaction B_m^{pl}, as described in [10, 11, 21, 29, 75, 77, 93]. To avoid confusion, we note that the dispersion relations given by (8.1), (8.8) and (8.9) are obtained for the 'open loop' system, which means

https://doi.org/10.1017/S0022377815001403 Published online by Cambridge University Press

$B_m^{er} + B_m^f = \text{const.}$ or zero. The feedback control is incorporated into the model though B_m^{ext} in (10.1), as described, for example, in [2, 10, 39, 41–45, 72, 76, 90, 95].

If Γ_m is found in some particular case, the main questions are whether it will remain the same at varying amplitude of $\boldsymbol{b}^{out}$ and fixed plasma parameters and if it will depend on γ or not?

The first question can be reformulated to whether the plasma reacts to $\boldsymbol{b}^{out}$ as a linear system? In view of the practical applications, this can be also discussed in terms of the mode rigidity [10, 17, 24, 40, 44, 73, 90, 93, 105, 106] which means the invariance of the mode structure in the plasma at fixed parameters of the equilibrium configuration during magnetic feedback stabilization and/or error field correction [105].

The linearity is one of the foundation principles of most stability theories. Its validity or relevance can be proved by experiment only. In the DIII-D tokamak, the linearity of the plasma response was found to be a good assumption for the externally applied resonant magnetic fields 10^{-4}–10^{-3} of the main toroidal field [75]. A linear plasma response to the applied error field was confirmed in both the JET and the Mega Ampère Spherical Tokamak (MAST) [107].

It is clear that such linearity cannot be expected just near the stability boundary. In [47, 48], the predictions of linear ideal MHD were compared with measurements of the external plasma response to applied $n = 1$ magnetic perturbations in rotating, H-mode discharges on the DIII-D tokamak. The plasma response calculated with the MARS-F code was found adequate to describe the plasma response for values of β_N up to approximately 75 % [47] or 80 % [48] of the no-wall stability limit $\beta_N^{no\,wall}$. It is interesting that, for higher plasma pressures, the ideal MHD model overestimated the perturbed field (by a factor of 1.5–3 [47]). This is actually good news because it means that, in this particular case, the plasma behaves better near the stability limit than is predicted by the ideal linear theory. At least, this does not compromise the linearity but rather indicates the increasing importance of stabilizing non-ideal effects [47].

With linear plasma response, the ratio B_m^{out}/B_m and, accordingly, g_m and Γ_m defined by (9.15) and (9.16) must be independent of B_m. In the following analysis of (8.8) and (8.9), we also assume that g_m does not depend on γ. Then (8.8) and (8.9) will give us the resolved dispersion relations with the right-hand sides depending on the plasma parameters only.

The latter assumption is naturally justified in the ideal MHD models for RWMs, where the plasma inertia is disregarded [10, 14, 19, 35, 38, 43, 44, 46, 49, 68–70, 73, 108] because RWMs are considered as slow modes. Indeed, if $\delta K = 0$ in (3.14) and the plasma is assumed ideal ($N = 0$), the flux F does not bring a dependence on γ in (8.10). For a non-ideal plasma, this will be true when $|N| \ll |F|$.

12. Separation of the plasma response from the magnetic signals

We have already mentioned that the plasma response can be measured. This was with references to the schemes based on the single-mode approach. The method, however, has a perfect theoretical background. Properly integrating the Maxwell equations over the volume V bounded by the toroidal surface S in the plasma–wall vacuum gap one obtains

$$\frac{1}{4\pi}\oint_s \left[(\boldsymbol{n}\times\boldsymbol{B})\times\frac{\boldsymbol{r}-\boldsymbol{r}_s}{|\boldsymbol{r}-\boldsymbol{r}_s|^3} + (\boldsymbol{n}\cdot\boldsymbol{B})\frac{\boldsymbol{r}-\boldsymbol{r}_s}{|\boldsymbol{r}-\boldsymbol{r}_s|^3}\right] \mathrm{d}S = \begin{cases} -\boldsymbol{B}^{out}(\boldsymbol{r}) & \text{if } \boldsymbol{r}\in V \\ \boldsymbol{B}^{pl}(\boldsymbol{r}) & \text{if } \boldsymbol{r}\notin V\cup S, \end{cases} \tag{12.1}$$

https://doi.org/10.1017/S0022377815001403 Published online by Cambridge University Press

where $\boldsymbol{r}$ is the observation point, $\boldsymbol{r}_s$ is the point at the surface S and $\boldsymbol{n}$ is the outward unit normal to S. This is a precise equality allowing the separation of the plasma-produced magnetic field $\boldsymbol{B}^{pl}$ from the total magnetic field $\boldsymbol{B} = \boldsymbol{B}^{pl} + \boldsymbol{B}^{out}$ [94]. If $\boldsymbol{n} \cdot \boldsymbol{B} = 0$, which happens when S coincides with a magnetic surface (for example, the plasma boundary), (12.1) gives the 'virtual casing principle' solution [109, 110]. Applications based on (12.1) or its equivalents are well known in the tasks of stellarator equilibrium [111].

With $\boldsymbol{B}$ expressed by (3.3), this can be divided on two equations, for $\boldsymbol{B}_0$ and $\boldsymbol{b}$. If the perturbation $\boldsymbol{b}$ could be measured or prescribed at the surface, then calculating the left-hand side of (12.1) we obtain both $\boldsymbol{b}^{pl}$ and $\boldsymbol{b}^{out}$.

Such application of the mathematically strict result will suffer from the incomplete information provided by the magnetic measurements at the integration surface S. The accuracy of the method based on the measured $\boldsymbol{b}$ can be improved by comparing $\boldsymbol{b}^{out}$ thus found from (12.1) against $\boldsymbol{b}^{out}$ precisely calculated by the Biot–Savart law with known currents in the external conductors.

In a full-scale experiment, only the field $\boldsymbol{b}^f$ from the correction or feedback coils may be known, which is a part of

$$\boldsymbol{b}^{out} = \boldsymbol{b}^w + \boldsymbol{b}^{er} + \boldsymbol{b}^f, \tag{12.2}$$

where $\boldsymbol{b}^w$ is the contribution due to the currents in the wall, and $\boldsymbol{b}^{er}$ describes the error field (usually unknown, but, presumably, static). In the single-mode case, when (12.2) reduces to (11.2), $\boldsymbol{b}^w$ and $\boldsymbol{b}^f$ have similar structure, which cannot be expected in a real experiment. Their difference and the dynamically evolving $\boldsymbol{b}^w$ itself can be evaluated by finding $\boldsymbol{b}^{out} - \boldsymbol{b}^f$ after integration in (12.1). Such extraction of $\boldsymbol{b}^w$ from the measured $\boldsymbol{b}$ can be used in experiments with a control of plasma stability against RWMs or ELMs, with probing the plasma with externally applied RMPs [10, 11, 21, 29, 47, 48, 75, 77, 93, 112] or in the test blanket module error field simulation experiments [113]. As a part of separation of different inputs to $\boldsymbol{b}$, knowledge of $\boldsymbol{b}^w$ could be useful for optimizing the spectrum of $\boldsymbol{b}^f$ and for improving the wall model.

Equation (12.1) is free from any assumption on the plasma because it is derived from the Maxwell equations only. Therefore, the diagnostics based on measurements of $\boldsymbol{b}$ combined with (12.1) can be a universal tool in testing various theoretical predictions and suggestions such as the linear plasma response and possible mode rigidity [10, 17, 24, 40, 106]. Equation (12.1) can also be used to complement the methods of detecting the approach to the stability boundary in tokamaks, stellarators and pinches.

Equations (3.1) and (3.2) describe the plasma dynamics in terms of full $\boldsymbol{b}$. Modelling of the experiments with RMPs or feedback control of plasma stability is always aimed at finding an optimal $\boldsymbol{b}^f$. This means $\boldsymbol{b}^f$ provoking a desired plasma reaction. With unlimited degrees of freedom, the problem becomes tractable when the main 'resonances' are established. In the CarMa code, that proved to be the best in RWM studies, the plasma response matrix is found by calculating the coupling of the linearly perturbed MHD equilibria and 3-D eddy current via the control surface method. This strategy is described in detail [69–71] as a sequence of actions. The separation of $\boldsymbol{b}^{pl}$ and $\boldsymbol{b}^{out}$ from $\boldsymbol{b} = \boldsymbol{b}^{pl} + \boldsymbol{b}^{out}$ performed in the CarMa is actually equivalent to and proved to be correct by (12.1) [94].

https://doi.org/10.1017/S0022377815001403 Published online by Cambridge University Press

13. Comparison of thin- and thick-wall predictions

Two different dispersion relations, (8.8) and (8.9), represent two asymptotes of (8.1). One is valid at $d_w \ll s$ and the other at $d_w \gg s$, which means, respectively, the wall thin or thick compared to the skin depth. It follows from (8.2) that

$$\frac{d_w}{s} = \mathrm{Re}\sqrt{\gamma\tau_{sk}}. \tag{13.1}$$

Accordingly, the modes with $d_w \ll s$ can be called slow RWMs, while the modes with $d_w \gg s$ are fast RWMs. This refers to $|\gamma|$ only irrespective of the origin of the mode. Then 'RWM' is a generic name indicating that the mode can dissipate its energy in the resistive wall. This can cover the conventional RWMs, tearing modes, ELM or disruption precursors and other modes that are detected by the magnetic probes in the plasma–wall vacuum gap.

The key quantity determining whether the mode should be qualified and treated as slow of fast RWM is $|\gamma|\tau_{sk}$. To be slow, the mode should have small growth (or decay) rate and small rotational frequency. The fast RWM may have either $|\gamma_R|$ or ω large. This means, in particular, that the modes with the same $\gamma_R\tau_{sk}$ but essentially different $\omega\tau_{sk}$ may belong to the different classes.

In the discussions of the 'conventional' RWMs, always τ_w is used as a characteristic time scale [10–25, 28–30, 35–46, 50–73], and the RWMs are described as the modes with γ_R of the order of $1/\tau_w$. Our analysis also includes faster modes. Then τ_{sk} becomes a more convenient parameter, as illustrated by the dispersion relations in the easily comparable compact forms of (8.8) and (8.9).

These two expressions give the same result at $g_m = 1$ corresponding to $s = d_w$. Strictly speaking, this lies in between the applicability regions of these relations ($s \gg d_w$ and $s \ll d_w$, respectively). However, it is numerically proved [89, 114–116] that (8.8) and (8.9) give quite accurate estimates of γ even in the intermediate range of s/d_w. This is illustrated by figure 5 for the locked modes, where the straight line corresponds to the thin-wall prediction by (8.8), the dashed-dotted parabolic line represents (8.9) and the solid curve shows $\gamma\tau_{sk}$ numerically found from the dispersion relation

$$g_m = \sqrt{\gamma\tau_{sk}}\frac{\mathrm{K}_{m-1}(y_i)\mathrm{I}_{m-1}(y_e) - \mathrm{I}_{m-1}(y_i)\mathrm{K}_{m-1}(y_e)}{\mathrm{K}_m(y_i)\mathrm{I}_{m-1}(y_e) + \mathrm{I}_m(y_i)\mathrm{K}_{m-1}(y_e)} \tag{13.2}$$

equivalent to (13) in [89] or to (32) in [114]. Here, I and K are the modified Bessel functions, y_i and y_e are the values of

$$y = \sqrt{\gamma\tau_{sk}}\frac{r}{d_w} \tag{13.3}$$

at the inner ($r = r_w$) and at the outer ($r = r_w + d_w$) sides of the wall so that $y_e - y_i = \sqrt{\gamma\tau_{sk}}$. It can be shown that (13.2) reduces to (8.8) at $s \gg d_w$ and to (8.9) at $s \ll d_w$.

Equation (13.2) is obtained in the cylindrical approximation by using (9.2) for the vacuum region and similar solution to (7.7) for the wall without expansion in radius or in s/d_w. Much simpler equations (8.8) and (8.9) are thin- and thick-wall asymptotes. Comparison with the results of toroidal calculations [116] proves that these cylindrical equations are quite reliable.

The upper curve in figure 5 smoothly connects the thin-wall and thick-wall regimes, while (8.8) and (8.9), if used behind their inherent limitations on g_m, will give us a sharper transition at $g_m = 1$ when $s = d_w$. This occurs at $\gamma = \gamma_l$ with $\gamma_l\tau_{sk} = 1$ or

$$\gamma_l\tau_w = r_w/d_w, \tag{13.4}$$

https://doi.org/10.1017/S0022377815001403 Published online by Cambridge University Press

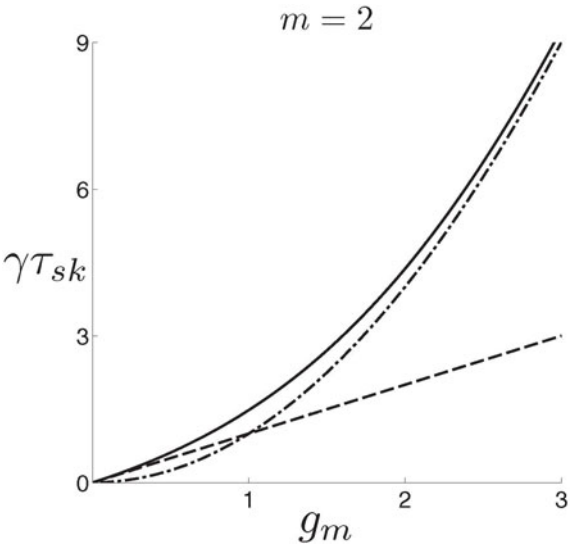


FIGURE 5. Calculated dependence of γ on g_m for the locked modes with $m = 2$ and the wall with $d_w/r_w = 0.02$. The solid line is the cylindrical result given by (13.2), the dashed line shows the thin-wall prediction by (8.8), while the dashed-dotted line corresponds to the thick-wall limit described by (8.9). (Figure 3 from [114]. Figure courtesy of Yanovskiy.)

where τ_w is introduced by (4.8). This simple formula can be used as a convenient definition of the point behind which the thin-wall evaluation of γ becomes less reliable than the thick-wall estimates. Both r_w/d_w and τ_w that define γ_l here are the parameters (at least, approximately) known for each device. Comparing the measured or calculated growth rate γ with γ_l one can easily decide whether or not the skin effect plays a role in the energy balance. Equation (13.4) gives the lower boundary for the fast non-rotating RWMs.

For the purely rotating modes (with $\gamma_R = 0$) we have from (13.1)

$$\frac{d_w}{s} = \sqrt{\frac{n\omega\tau_{sk}}{2}}. \tag{13.5}$$

If $d_w/s \gg 1$, this regime must be described by (8.9) implying that

$$g_m = (1 + i)d_w/s \tag{13.6}$$

in this particular case. With this g_m, the thin-wall dispersion relation (8.8) predicts quite severe instability with $\mathrm{Re}\gamma^{sh}\tau_{sk} = d_w/s$ in obvious contradiction to the initial assumption that $\gamma_R = 0$. This dramatic disagreement in the predictions of (8.8) and (8.9) is much more serious than a qualitative difference in γ of the order of 30 % at $d_w = s$ in figure 5 for the modes with $\omega = 0$. It shows that these two approaches may lead to essentially different conclusions on the stability boundaries for the rotating modes.

14. Application of simple RWM models to real devices

Equations (13.4) and (13.5) suggest that the choice between the two possibilities (thin- or thick-wall modelling) depends on r_w/d_w, if the RWM dynamics is described in terms of $\gamma\tau_w$ or $\omega\tau_w$.

https://doi.org/10.1017/S0022377815001403 Published online by Cambridge University Press

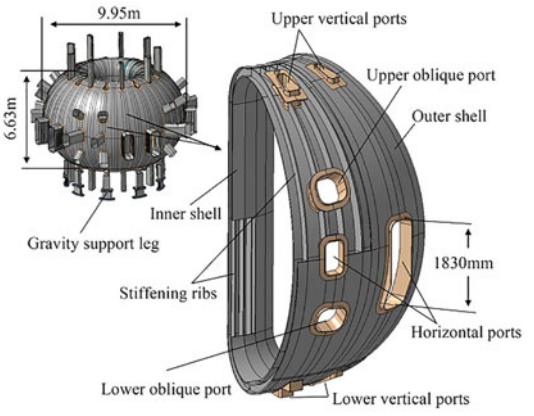


FIGURE 6. The JT-60SA vacuum vessel. The left part shows the overall structure, and the right part is the view of its 10-degree segment. (Figure 1 from [117].)

While r_w/d_w naturally appears as a key parameter in our analysis, it is difficult (or even impossible) to find this ratio in papers on plasma stability. The walls are usually non-circular. Also, their thickness is not a constant, the conductivity is not uniform, they have cuts and ports. An example is shown in figure 6 (from the paper [117] on manufacturing and development of JT-60SA vacuum vessel and divertor). Ambiguity in the definitions of r_w and d_w and other parameters of interest is an attribute of all models representing a real device in a simplified form. This extends even to the majority of stability codes. For example, the walls are often treated as axisymmetric and poloidally continuous [49, 76, 78, 88, 108, 116, 118–121]. Sometimes, the 2-D wall approximation is qualitatively not good enough to describe even the wall response itself (i.e. in the absence of the plasma) [108]. On the other hand, it is known that a much simpler single-mode cylindrical model can give quite reliable forecasts with good agreement with experimental and numerical results [2, 10, 12, 15, 41, 57, 75, 76, 95]. This is true, in particular, with respect to (8.8) and (8.9) the predictions of which are numerically proved correct [114–116], as illustrated in figure 5.

Though the wall parameters r_w and d_w can be only introduced in some average sense, their use facilitates estimates and comparisons of different toroidal plasma devices. Information on some of them is collected in table 1. Here, the data for J-TEXT are taken from [122], for JFT-2M from [123], for DIII-D from [13], for LHD from [46], for JET from [1] and [124], for RFX-mod from [106, 120] and for EXTRAP T2R from [39, 125, 126].

The numbers for ITER represent the model used in [72]. The wall radius for JT-60SA in table 1 corresponds to $r_w = 1.2a$ (consistent with calculations in [49]) with plasma minor radius $a = 118$ cm [26], and the wall thickness is taken from [27]. Both ITER and JT-60SA tokamaks will have a double wall [2, 27, 72, 117]. In such cases, a thin-wall dispersion relation will be different from (8.8), as discussed in [72, 127]. However, the second wall cannot affect the RWM dynamics at strong skin effect in the nearest conductor. This allows us to use (13.4) and (13.5) as practical estimates.

These equations and table 1 allow us to conclude that the thin- to thick-wall transition in the DIII-D tokamak should be expected at $\gamma\tau_w$ or $\omega\tau_w$, smaller by factor of 4–5 than in the reversed field pinch devices RFX-mod and EXTRAP T2R. From a theoretical viewpoint, large values of r_w/d_w in RFX-mod and EXTRAP T2R indicate

https://doi.org/10.1017/S0022377815001403 Published online by Cambridge University Press

Device	J-TEXT	JFT-2M	DIII-D	JT-60SA	ITER	LHD	JET	RFX-mod	EXTRAP T2R
Wall minor radius r_w (cm)	33.5	37.5	80	141.6	472.5	120	130	51.3	19.8
Wall thickness d_w (cm)	1.6	1	1.9	1.8	6	1.5	1.2	0.3	0.1
Ratio r_w/d_w	20.9	37.5	42	78.7	78.8	80	108	171	198

TABLE 1. The wall parameters r_w and d_w for different toroidal plasma devices.

that the thin-wall approximation must be good for these devices up to high $\gamma\tau_w$. On the contrary, smaller r_w/d_w in DIII-D points to the necessity of considering the thick-wall effects at $\gamma\tau_w$ or $\omega\tau_w$ of order 40 and higher.

This should be compared to $\gamma\tau_w = 30$, the level where the calculations demonstrated the ability of the DIII-D feedback system of the RWM suppression [10, 38, 43]. Our analysis confirms that the thin-wall modelling in such cases is justified for DIII-D, though its validity is already marginal.

It is interesting to note the same values of r_w/d_w in ITER and JT-60SA despite the differences in the dimensions and the wall parameters. This similarity means that the ITER predictions for RWMs can be easily transformed to JT-60SA even without rescaling of $\gamma\tau_w$ or $\omega\tau_w$.

It could be tempting to exploit the LHD nearness to ITER and JT-60SA on the r_w/d_w scale. However, because of the helical structure of the LHD wall, the comparison cannot be as straightforward as between two tokamaks.

To apply simple models to real devices, we need τ_w. The data on τ_w show sometimes a scatter by a factor of 2–3 or larger, as discussed in [93]. In [10], for example, τ_w in DIII-D is estimated as 5 ms and τ_w in JET as 3 ms. In [21], the characteristic decay time of a predominantly $m = 1$ eddy-current pattern is given as 7 ms for DIII-D and 6.3 ms for JET. In the latter case, the mentioned wall time may be different from τ_w defined by (4.8). For JT-60U, this formula gives $\tau_w \approx 10$ ms [25]. In ITER, τ_w is estimated as 0.3 s [72, 76]. In [56], where the RWM simulations have been performed with the hybrid kinetic-MHD code MARS-K, the longest $n = 1$ eddy-current decay time of the ITER double vacuum vessel was found to be approximately 0.4 s.

Even when the wall has an intricate shape far from the cylindrical image, one can introduce some physically reasonable τ_w. In [46] the calculated 'wall time' in LHD was $\tau_w = 31.5$ ms. For the Alcator C-Mod tokamak, $\tau_{sk} = 4.2 \times 10^{-4}$ s (instead of τ_w depending on r_w) was given in [128].

In principle, it must be possible to determine τ_w by measuring the vacuum vessel responses to perturbations [10, 75, 93]. This also gives some scatter. For example, it is stated in [73] that the presence of the plasma modifies the time response of the shell currents by reducing it from $\tau_w \approx 6$ ms for a very small plasma to $\tau_w \approx 3.5$ ms for a fully-developed plasma in the DIII-D. This is, probably, because the perturbation structure is different in these two cases.

It is well known that the thin-wall approach should be used for slow modes only. This, however, is not always mentioned in applications, especially when the numerical results are described. There are many codes based on the thin-wall approximation, including KINX [44, 129], VALEN [41], GATO–VACUUM [73], DCON–VACUUM

https://doi.org/10.1017/S0022377815001403 Published online by Cambridge University Press

or NMA [10, 43], modified KSTEP [46], CASTOR_FLOW [78], STARWALL [68], MARS [56, 108, 118] and MINERVA/RWMaC [49]. As illustrated by figure 5, their predictions can be reliable at small $\gamma\tau_w$, but sometimes the calculations show $\gamma\tau_w > r_w/d_w$. For example, in [41] the results are presented up to $\gamma\tau_w = 100$ for the DIII-D tokamak, while in [49] the thin-wall modelling of RWM dynamics in the JT-60SA tokamak was performed with $\gamma\tau_w$ reaching 80. In [82], the VALEN computational results are shown with a growth rate of 10^4–10^5 s^{-1} while the open loop growth rate of the RWM was estimated as 10^3 s^{-1}. In [119], the wall forces produced during ITER disruptions have been calculated up to $\gamma\tau_w = 1000$ still using a thin-conducting-wall model. In all these cases, the results must be different if the skin effect is properly included.

15. Rotational stabilization in the thick-wall limit

In the example with g_m given by (13.6), the mode unstable at $d_w \ll s$ becomes marginally stable at $d_w \gg s$. This favourable tendency clearly seen in (8.8) and (8.9) is a consequence of larger energy dissipation in the wall when the skin effect is combined with fast rotation of the mode. Now we consider it in more detail.

With γ introduced by (2.2) and g_m in the form

$$g_m = g_R + \mathrm{i}g_I \tag{15.1}$$

with real g_R and g_I, (8.9) reduces to

$$n\omega\tau_{sk} = 2g_R g_I, \tag{15.2}$$

where $\omega = \gamma_I/n$ is the toroidal rotation frequency of the mode, and

$$\gamma_R = (g_R^2 - g_I^2)/\tau_{sk} = \gamma_R^{ld}(1 - \omega^2/\omega_{cr}^2). \tag{15.3}$$

In the latter expression, γ_R^{ld} and ω_{cr} are related to the plasma parameters through

$$\gamma_R^{ld} = \frac{n}{2}\omega_{cr} = g_R^2/\tau_{sk}. \tag{15.4}$$

It is clear from (15.3) that γ_R^{ld} is the growth rate at $\omega = 0$, or when the mode becomes locked. The other constant ω_{cr} gives the angular frequency at which $\gamma_R = 0$.

Equation (15.3) explicitly shows that the real growth rate γ_R decreases when the mode rotates faster. The modes unstable at $\omega < \omega_{cr}$ become stable at $\omega > \omega_{cr}$. This beneficial effect, leading to $\gamma_R < 0$ at the mode rotation above the critical level ω_{cr}, has a full right to be called rotational stabilization, in addition to several other candidates proposed earlier [10] for explanation of the experimental results. The difference and advantage of our approach is that we derived (15.3) from the first-principle equations describing the electromagnetic interaction. This guarantees that the effect predicted by (15.3) must be robust whenever we enter the region of fast RWMs, irrespective of their origin.

We derived this equation assuming $s/d_w \ll 1$, but it can be used at a weaker restriction $s/d_w < 1$ [115, 130]. This is confirmed by the numerical solution of (13.2). The calculated dependence of g_R on g_I at the stability boundary ($\gamma_R = 0$) of the $m = 2$ mode is presented in figure 7. Equation (15.3) predicts that this curve must be approximated by the straight line $g_I = g_R$ at large g_R. Actually, the deviation from this line is less than 10 % at $g_R > 1.5$. This also corroborates the main result and

https://doi.org/10.1017/S0022377815001403 Published online by Cambridge University Press

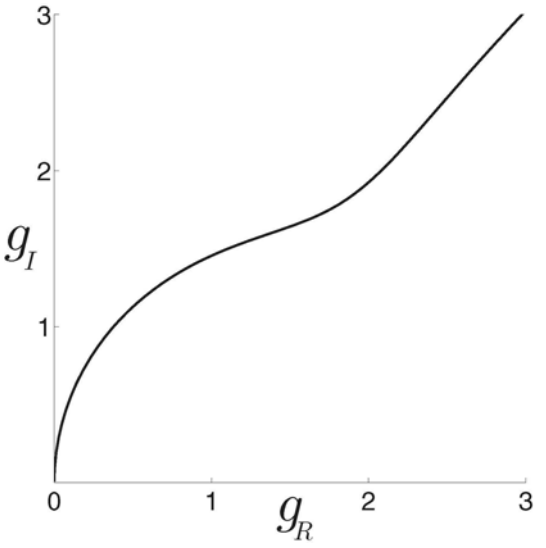


FIGURE 7. Dependence of g_R on g_I at the stability boundary ($\gamma_R = 0$) of the $m = 2$ mode. (Figure 1 from [115]. Figure courtesy of Yanovskiy.)

conclusions of [65–67] and proves that they remain valid at smaller g_R and g_I than allowed by the expansions in $s/d_w \ll 1$ employed on the way to (15.3).

In figure 8, dependence (15.3) shown by the dashed parabolas is compared with precise solutions of the cylindrical dispersion relations with the ferromagnetic effect accounted for [86]. The numbers attached to the curves indicate the magnetic permeability of the wall. In the lowest pair representing the wall with $\mu = 1$, the solid curve is the solution of (13.2). One can see good agreement between strict (13.2) and asymptotic (15.3) results.

The dispersion relation (15.3) connects two measurable quantities, γ_R and ω. Its simplicity suggests easy experimental testing of the discussed model. It contains two parameters, γ_R^{ld} and ω_{cr}. According to (15.4), $2\gamma_R^{ld} = n\omega_{cr}$. This relation is free from other unknowns and ready for comparison with measured ω_{cr}, which is the mode ω at the stability threshold, and the mode growth rate after the rotation braking. As shown in figure 9, this linear dependence looks quite reliable compared to the solution from (13.2).

The regime considered here is in between the thin wall and ideal-wall limits, and the electromagnetic interaction of the mode with a nearby resistive wall, providing the energy dissipation, is an essential element of the process. Accordingly, this rotational stabilization should be described differently from the customary simplified interpretations [1, 12, 17, 23, 32, 35–40, 131–133].

The proposal in [1], for example, was that if the mode rotation is fast compared with the wall time, the magnetic perturbation of such a mode does not have time to penetrate the wall. Then the wall appears as an ideal conductor, and the plasma modes are wall stabilized. In [36] it was stated that as the rotation frequency becomes larger than the inverse wall time, the resistive wall behaves like a superconducting wall and the mode is stabilized (ac wall stabilization). Similar arguments have been used in interpretations of the experimental results in DIII-D [23] and EXTRAP T2R [39]. Our analysis shows that, contrary to these opinions, even at $\omega\tau_w \gg 1$ the energy

https://doi.org/10.1017/S0022377815001403 Published online by Cambridge University Press

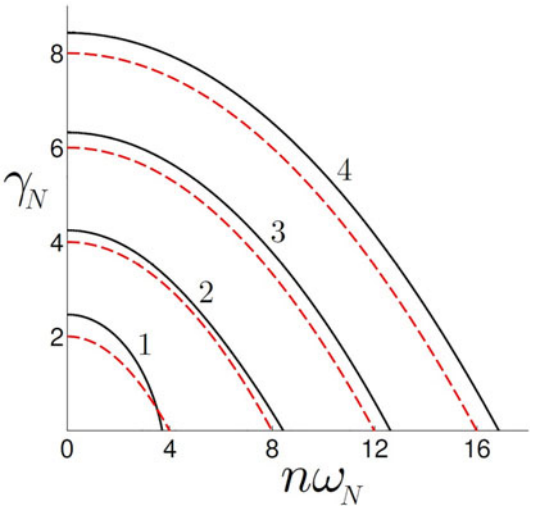


FIGURE 8. The calculated dependences of the growth rate γ_R on the angular frequency $n\omega$ normalized to τ_{sk} for the mode with $m=2$ at fixed $g_R=\sqrt{2}$ and varying g_I and the walls with $r_w/d_w=50$ and magnetic permeability μ from 1 to 4, shown above the curves. The solid curves are calculated by the ferromagnetic equivalent of (13.2) (see (4)–(6) in [86]) and the dashed parabolas by formula (15.3) with τ_{sk} replaced by τ_{sk}/μ. (Figure 6*a* from [86]. Figure courtesy by Yanovskiy.)

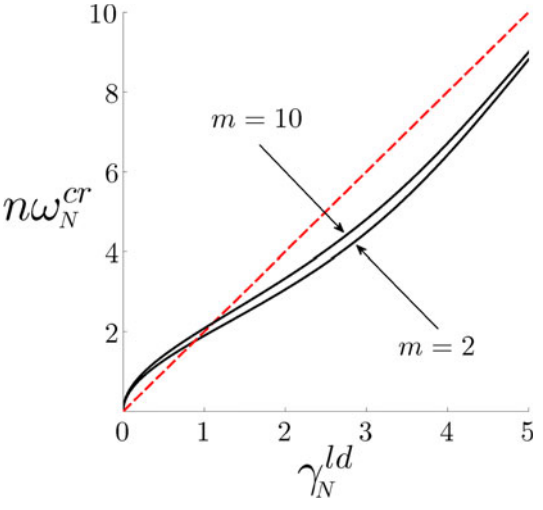


FIGURE 9. Normalized critical angular frequency $n\omega_N^{cr}\equiv n\omega_{cr}\tau_{sk}$ (at $\gamma_R=0$) versus $\gamma_N^{ld}\equiv\gamma_R^{ld}\tau_{sk}$ (the normalized growth rate of the same mode when it becomes locked) for the $m=2$ and $m=10$ modes. The solid curves are calculated by precise formula (13.2) and the dashed line by formula (15.4). (Figure 6 from [130]. Figure courtesy by Yanovskiy.)

sink because of the wall resistivity should be accounted for in the energy balance. Finally, the wall does not behave as an ideal conductor, but, nevertheless, provides the rotational stabilization.

https://doi.org/10.1017/S0022377815001403 Published online by Cambridge University Press

There are also statements that the plasma rotation relative to the wall can result in the plasma 'seeing' the wall as perfectly conducting, because of the skin effect [37, 38]. These comments appeared in discussions of the RWM physics which means a moderate level of rotation. It follows from our estimates that in such cases, the skin effect does not make the wall ideal. In other words, we propose another stabilizing mechanism.

Stabilization in (15.3) appears because of the skin effect related to the mode rotation. Their interplay at the stability boundary ($\gamma_R = 0$) is illustrated by (13.5). The role of the mode rotation is explicitly shown in (15.3), and the skin effect is the reason why (8.8) and (8.9) are different. If the skin effect is disregarded, (8.8) gives us, instead of (15.3), $\gamma_R \tau_{sk} = g_R$ independent of the mode rotation and always (but incorrectly at $s < d_w$) indicating instability at positive g_R.

In (15.3), the stabilizing effect is related to the mode rotation. In the RWM research, the rotational stabilization is usually discussed in terms of the plasma rotation [2, 10–24, 28–30, 32–34, 36–38, 43, 45, 49–64, 75, 96–100, 105, 108, 118]. Experiments show that, to be effective, the plasma toroidal rotation speed should exceed a critical value. Despite a number of efforts, a self-consistent, experimentally validated theoretical model for predicting the stability threshold of the RWM and its dependence on the plasma rotation has not yet been developed [10].

This is because of two reasons. First, the problem of plasma rotation in tokamaks is still in a state where the sources and sinks in the integral torque balance remain to be established [92, 134, 135]. This is explained by the fact that the plasma is an open system expelling the momentum and energy outwards in an uncontrolled manner. These losses depend not only on the equilibrium parameters, but on the spectrum and intensity of the developed MHD activity. Second, there is no yet a reliable theory relating the mode frequency ω to the plasma parameters.

16. Ideal versus non-ideal MHD

The most developed and widely used for tokamaks and stellarators is the ideal MHD. With $N = 0$, (3.14) will give us real F because of the self-adjointness of the ideal MHD operator originating from (3.2) [3–8]. This property cannot be spoiled by the resistive dissipation in the wall, as discussed in [10, 38, 43, 46], though in the thin-wall approximation. With real F, (4.1) or (8.1) give real γ. The fact that the ideal MHD with a resistive wall leads to slowly growing modes with zero real frequency ($\omega = 0$) was emphasized in [35]. To discuss the case described by (2.2) and (15.1)–(15.3) with $\omega \neq 0$ we need a complex F. This can be generated by some $N \neq 0$ in (3.14), which requires a step beyond the bounds of static ideal MHD.

Such extensions are usually explained as incorporating some dissipation or non-ideal MHD effects and plasma rotation [2, 10–16, 18–21, 23, 25, 28, 29, 32–38, 40, 45, 50–64, 75, 100, 118, 133, 136–143]. This brings a variety of possibilities. For example, the dissipation can be introduced by allowing the plasma viscosity [10, 32, 40, 141] and/or resistivity [10, 101, 142]. Other options include the mode resonances with stable waves (such as Alfvén waves or sound waves), with the magnetic precession drifts of trapped thermal ions and electrons or with trapped energetic particles [36, 140–143]. Further improvements of such advanced models can be done by allowing for anisotropy of the equilibrium pressure, the perturbed electrostatic potential, the radial excursion of particle trajectories, the finite Larmor radius corrections to the particle orbit [55], etc. In addition, the halo currents outside the main plasma, two fluid effects and the presence of stochastic regions surrounding

https://doi.org/10.1017/S0022377815001403 Published online by Cambridge University Press

the confined plasma have been considered [10]. Finally, turbulence and anomalous processes are also mentioned in the RWM studies [10, 16, 45, 56, 58]. And this is not the end because we have not yet listed the interaction of RWMs with other modes (ELMs or fishbones [10, 23, 24, 112, 144]) and the error fields playing an important role in instability triggering.

Starting from (3.4), such mechanisms are symbolically represented by N that can be calculated if $\boldsymbol{N}$ in (2.4), Ohm's law and the equation of state were prescribed. Incorporation of non-ideal effects is necessary if the equation

$$\delta K + W_p + W_s + W_g + W_w + W_{w+} = -(D_w + N), \tag{16.1}$$

a combination of (3.14) and (4.1), with $N = 0$ cannot describe the observed phenomena. In particular, the rotational stabilization predicted by (15.3) requires $\omega \neq 0$ which may be possible if N gives a noticeable imaginary contribution into (16.1).

This means a toroidally rotating mode in real experiments. As a rule, the origin of this rotation and the relation of ω to the plasma parameters are not precisely known (for the reasons mentioned above), but the knowledge of $\omega \neq 0$ from the magnetic measurements can be used as a replacement of the missing part of the theory. The measured $\omega \neq 0$ and additional measurements of the plasma response can give enough information for testing the predictions of (15.3) and evaluation of the right-hand side in (16.1).

With too many uncertainties, a justified choice of a dissipation mechanism in the plasma requires either convincing experimental identification or indisputable theoretical arguments. Equation (16.1) shows that an initial step must be elucidation of the energy and momentum losses outside the plasma. These can be disregarded if D_w is small and the wall behaves as either ideal or 'at infinity'. If not, and the wall is the main outer sink, D_w must be an obligatory part of calculations with clear understanding that its contribution to (16.1) can be essentially different from the thin-wall estimates.

The widely used notions 'kinetic model' or 'kinetic approach' [2, 10, 53, 56, 57, 61–64, 108, 118, 136, 137, 140, 141, 143] actually refer to some particular interaction of the plasma with either waves or particles. Though some agreement with experiments is reported, it is often clear that real plasma dynamics does not precisely follow the scenarios prescribed by the available models. One can add that, contrary to the mathematically perfect ideal MHD stability model [3–8], the kinetic approaches are still very much in a state of development.

17. Slow RWMs, fast RWMs and ideal MHD modes

It is well known that the growth rate of conventional (slow) RWMs is several orders of magnitude smaller than that of ideal kink modes [35, 41, 46, 68, 78, 118]. This is related to the essential difference between the wall time τ_w and the Alfvén time τ_A. In the existing devices, τ_A are microseconds or even smaller, while τ_w are several milliseconds [10, 21, 46, 75]. For example, $\tau_w = 10^4\tau_A$ was assumed in calculations in [55]. For ITER, the choice was $\tau_w = 6.2 \times 10^5\tau_A$ [56]. In [49], the RWM stability for JT-60SA was analysed with $\tau_w = 3 \times 10^3\tau_A$.

In the analytical models, slow RWMs are formally defined as the modes with $s \gg d_w$. As shown in figures 5 and 7, this can be extended to a wider region with $s > d_w$. Then the opposite $s < d_w$ determines fast RWMs with growth rates and rotation frequencies, roughly, 50–100 times higher than those of slow RWMs. The boundary $s = d_w$ between them is given by (13.4) for the locked modes.

https://doi.org/10.1017/S0022377815001403 Published online by Cambridge University Press

The modes can be called RWMs as long as their dynamics is affected by the resistive dissipation in the wall. This must be the case when D_w is larger than δK in the energy balance (16.1).

According to (3.5),

$$\delta K = \gamma^2 K_0 \tag{17.1}$$

with K_0 given by (6.2), while

$$D_w = \gamma \tau_w \frac{s}{2d_w} D_0^{sh} = \frac{\gamma \tau_w}{2\,\mathrm{Re}\sqrt{\gamma \tau_{sk}}} D_0^{sh} \tag{17.2}$$

at $s \ll d_w$, which is a consequence of (4.7), (4.10), (8.3), and (13.1). Both K_0 and D_0^{sh} defined by (4.9) and estimated by (9.12) are determined by the mode structure. Therefore, (17.1) and (17.2) show explicit dependence of δK and D_w on γ.

The mass density ρ_0 of the fusion plasma is very small, of the order of 10^{-10} g cm^{-3}. That is why K_0 (obtained by integration of $\rho_0|\boldsymbol{\xi}|^2$ over the plasma volume) is small, and δK is disregarded in the theory of conventional RWMs. Being much smaller than D_w at $s > d_w$, δK grows faster than D_w with increasing γ and decreasing s/d_w. The point where δK reaches the level of D_w can be considered as the upper boundary of the fast RWM range. Higher γ will make $\delta K > D_w$, which is the region $s/d_w \to 0$ where the wall can be treated as ideal.

If the transition from fast RWMs to the ideal kink modes occurs at $\gamma \tau_A = \varepsilon_{th}$, the estimate of the upper limit for the fast RWM growth rates will be

$$\gamma_{up} \tau_{sk} = \varepsilon_{th} \frac{\tau_{sk}}{\tau_A} = \varepsilon_{th} \frac{\tau_w}{\tau_A} \frac{d_w}{r_w}. \tag{17.3}$$

This should be compared to $\gamma_l \tau_{sk} = 1$ at the lower boundary, see (13.4). With $r_w/d_w = 50$ and the threshold level $\varepsilon_{th} = 1/20$ we have $\gamma_{up}\tau_{sk} = 3$ at $\tau_w = 3 \times 10^3 \tau_A$ or $\gamma_{up}\tau_{sk} = 10$ at $\tau_w = 10^4 \tau_A$. With $\tau_w = 6.2 \times 10^5 \tau_A$, as in [56], ITER-like $r_w/d_w = 80$ and quite small $\varepsilon_{th} = 1/200$ (17.3) gives us $\gamma_{up}\tau_{sk} = 39$.

These estimates show that the range of the fast RWMs between the slow RWMs and the ideal modes can be quite broad. This area is not yet properly explored in the theory because too many mechanisms can be involved in the torque–energy transfer in the perturbed state in tokamaks [1, 2, 9, 10, 25, 52–64, 92, 108, 118, 134–145]. To distinguish between them, one has to separate the sinks and sources of the momentum and energy. From various unknowns, the wall influence on the plasma dynamics must be the easiest to evaluate with codes such as CarMa [69–71, 108, 116, 118, 120, 121], taking rigorous account of the skin effect and 3-D features of the conducting structures surrounding the plasma.

The other codes for stability analysis of RWMs treat the wall as a magnetically thin shell. It must be noted that, with rare exceptions, the models behind the RWM codes may contain additional simplifications, albeit without mentioning and explanation of the ensuing consequences in applications. Typical examples are a single-mode approximation in the VALEN code [41] or the use of the trial function [35]

$$\boldsymbol{b} = c_{no}\boldsymbol{b}_{no} + (1 - c_{no})\boldsymbol{b}_{id} \tag{17.4}$$

for $\boldsymbol{b}$ in the plasma–wall gap and

$$\boldsymbol{b} = c_{no}\boldsymbol{b}_{no} \tag{17.5}$$

behind the wall with $\boldsymbol{b}_{no}$ and $\boldsymbol{b}_{id}$ the no-wall and ideal-wall solutions for $\boldsymbol{b}$ outside the plasma,

$$c_{no} = \frac{1}{1 + \gamma \tau_D} \tag{17.6}$$

https://doi.org/10.1017/S0022377815001403 Published online by Cambridge University Press

and τ_D a 'wall constant' expressed in the cylindrical limit as

$$\tau_D = \frac{1 - x_{pl}^{2m}}{2m}\tau_w, \tag{17.7}$$

where τ_w is defined by (4.8), $x_{pl} \equiv r_{pl}/r_w$ and r_{pl} the plasma minor radius (for derivations and explanations see [146]).

It was shown in [35], and confirmed in [146], that for the ideal toroidal plasma and slow RWMs described by (17.4) and (17.5) in the outer region, the energy principle yields the dispersion relation

$$\gamma\tau_D = -\frac{W_\infty}{W_b}, \tag{17.8}$$

where γ is the growth rate, W_∞ and W_b are the perturbed energies (the left-hand side of (16.1) at $\delta K = 0$) without and with an ideal wall. For a non-ideal plasma this is replaced by [36, 52, 55–58, 60, 61, 63, 64, 108, 118, 136–143]

$$\gamma\tau_D = -\frac{W_\infty + \delta W_k}{W_b + \delta W_k}, \tag{17.9}$$

where δW_k is the so-called 'kinetic contribution to the potential energy evaluated using the fluid RWM eigenfunction' [10] or, briefly, 'the kinetic term' [140].

At proper constraints, (17.9) must be a consequence of (16.1), and δW_k must be equal to $N + W_s$ in (16.1). The reduction of (16.1)–(17.9) can be done by the algorithm described in [146], but now with $N \neq 0$. It is clear that the resulting δW_k will depend not only on $\boldsymbol{N}$ in (2.4), but on the equation of state and Ohm's law. A justified choice of δW_k for a tokamak plasma is still an open question.

More often [55, 57, 61, 64, 108, 118, 136, 137, 139–141, 143] than not [36, 56, 58, 60, 63, 138, 142] (17.9) is used with verbal descriptions of τ_D such as 'characteristic resistive decay time for currents in the wall induced by the RWM' [136], 'magnetic penetration time of a resistive wall' [137], 'wall time of a resistive wall' [139], 'current decay time in the resistive wall' [140], 'characteristic wall time' [141], 'wall time constant' [143], and similar wordings. The use of such vague notions instead of precise definitions of τ_D in [35, 146] or, at least, its approximation (17.7) is confusing and inevitably leads to mistakes in applications. The most 'natural' one is a replacement of τ_D by τ_w [10, 140, 143]. For example, equations (15) and (C.12) in the famous review [10], otherwise equivalent to our (17.9), contain τ_w precisely defined by (4.8). However, τ_D and such τ_w are essentially different. For example, for $x_{pl} = 0.88$ at $m = 2$ we have $\tau_D = 0.1\tau_w$. For higher-m modes the ratio τ_D/τ_w will be yet smaller.

In [36, 56, 58, 60, 63, 138, 142], (17.9) is used with τ_D given by (17.7). This is the cylindrical approximation, as well as the trial function (17.4) itself. Therefore, even with 'correct' τ_D (17.9) can serve for estimates only, as implied by its derivation and mentioned in the original paper [35].

The algorithm of reducing of (16.1) with $N = 0$ to thin-wall ($s \gg d_w$) relation (17.8) is described in full detail in [146]. It is also shown there that in the thick-wall limit ($s \ll d_w$) a more correct estimate than (17.8) is

$$\gamma\tau_D = \frac{\tau_{sk}}{\tau_D}\left(\frac{W_\infty}{W_b}\right)^2, \tag{17.10}$$

which differs from (17.8) exactly as (8.9) from (8.8).

https://doi.org/10.1017/S0022377815001403 Published online by Cambridge University Press

It is tempting to say that (17.8) and (17.10) are equivalent, respectively, to (8.8) and (8.9). However, the latter two are valid for any plasma, but (17.8) and (17.10) are derived for an ideal plasma. On the other hand, (8.8) and (8.9) originally appeared as cylindrical (though here with (8.10) they are perfectly toroidal), but derivation of (17.8) and (17.10) with precisely calculated W_∞ and W_b was initially aimed at application with toroidal codes. This intention is spoiled by the use of (17.4) outside the plasma and τ_D in the form of (17.7).

Applicability of the popular estimate (17.9) with $\delta W_k \neq 0$ is restricted by the same $s > d_w$ as other thin-wall equations. It is not yet shown directly from (16.1), but the algorithm in [146] and similarity of the starting equations suggest that for the fast RWMs ($s < d_w$) we should use instead

$$\gamma \tau_D = \frac{\tau_{sk}}{\tau_D} \left(\frac{W_\infty + \delta W_k}{W_b + \delta W_k} \right)^2 . \tag{17.11}$$

It looks similar to (8.9) with complex g_m, though restricted by the use of the trial function (17.4) for $\boldsymbol{b}$ outside the plasma, which is an inherent element of the Haney–Freidberg approach resulting in (17.8) and (17.9) [35, 146]. A more general algorithm for reducing the energy principle to a simpler form can be proposed [147] for the cases when either $\boldsymbol{b} \to \boldsymbol{b}_{no}$ or $\boldsymbol{b} \to \boldsymbol{b}_{id}$. This means, respectively, the regions near the no-wall stability limit or near the ideal-wall stability limit. In the latter case, calculating the 'external' terms in the linear approximation in $\boldsymbol{b} - \boldsymbol{b}_{id}$ we obtain from (16.1) a dispersion relation [147]

$$\gamma^2 K_0 + (W_p + W_g^{id}) + N + W_s = \frac{d_w}{2\sqrt{\gamma \tau_{sk}}} \oint_{wall-} |\boldsymbol{b}_{id}|^2 \, \mathrm{d}S_w, \tag{17.12}$$

where W_g^{id} is W_g at $\boldsymbol{b} = \boldsymbol{b}_{id}$. Equation (17.12) provides a smooth transition from the fast RWMs described by disregarding $\gamma^2 K_0$ to the ideal modes when $\boldsymbol{b} \to \boldsymbol{b}_{id}$ and the right-hand side becomes negligible compared to $\gamma^2 K_0$. It allows to use the developed ideal-wall codes for stability analysis of RWMs near the traditional ideal-wall stability limit. Note that, contrary to (17.8)–(17.11), (17.12) is valid for a plasma of arbitrary shape and toroidicity.

18. Fast rotating modes in experiments

Complete theoretical analysis of such modes would involve a full cycle of MHD calculations with a reliable plasma model, which selection and justification is a separate problem. Before starting this hard work, one has to be sure that such efforts are worthwhile. The best motivation comes from experiments showing us a variety of the events with features of the fast RWMs.

A good example was described in [128] where τ_{sk} was estimated as 4.2×10^{-4} s for the wall in Alcator C-Mod tokamak and it was explicitly stated that fluctuations faster than this timescale, i.e. with a frequency greater than 375 Hz, experience 'thick' walls. Such were the observed tearing mode with 4.5 kHz and snake with 0.8 kHz.

This is an exceptional case where the data have been compared with thin-wall and thick-wall estimates with a clear conclusion that a thick-wall approximation is more appropriate [128]. Looking under this angle on other rotating perturbations often observed in a stable plasma, we can easily find a lot of different fast RWMs. The

https://doi.org/10.1017/S0022377815001403 Published online by Cambridge University Press

practical selection criterion to this class is $d_w/s > 1$. For steady-state rotating modes we can use (13.5) which can be rewritten as

$$d_w/s = \sqrt{\omega/\omega_l} = \sqrt{\nu/\nu_l}, \tag{18.1}$$

where $\omega_l = 2\pi\nu_l$ is defined by

$$n\omega_l\tau_{sk} = 2, \tag{18.2}$$

ν is the frequency of the measurable magnetic signal and τ_{sk} is related to τ_w by (8.7). Since $\nu = \nu_l$ (or $\omega = \omega_l$) gives $d_w/s = 1$, this can serve as a lower estimate for ν (or ω) providing a noticeable skin effect.

With $\tau_w = 5$ ms and $r_w/d_w = 50$, approximately corresponding to the DIII-D parameters, a rough estimate for the $n = 1$ mode will be $\nu_l = 3$ kHz. This is a reasonable number. For comparison, in the DIII-D experiments on the plasma response to externally applied non-axisymmetric fields [48], small amplitude tearing modes were observed on the magnetic diagnostics at frequencies >35 kHz. In other DIII-D experiments [17], the mode rotating with a frequency of 10 kHz was driven when β_N reached β_N^{wall}. Then it was expected that the vacuum vessel should act as an ideal wall in this frequency range. Our estimates show that the resistive dissipation in the wall can still be important for such modes, whereas the transition to the ideal-wall limit must be at higher frequencies. Even at 50 kHz we have quite modest $d_w/s \approx 4$ in the DIII-D. Much larger ratios of d_w/s can be inferred for a weakly coherent edge MHD mode at frequency approximately 100–300 kHz that accompanied the transition from L-mode to I-mode in the Alcator C-Mod plasma [148]. In such cases, the ideal wall approximation seems acceptable.

It is easy to find the opposite examples, the phenomena when the mode rotation is insufficient for resistive wall stabilization. In the DIII-D discharges described in [23], the $n = 1$ tearing modes appeared as the plasma rotation approached the minimum for the RWM stability. At the typical mode rotation frequencies of $\geqslant$1 kHz these modes were unstable. It was stated that at such frequencies the wall provides the same stabilizing influence as an ideally conducting wall [23]. However, (18.1) tells us that at 1 kHz the DIII-D wall must behave as resistive with a weak skin effect.

When the measured ω is larger than ω_l, the mode properties should be compared with predictions of (15.3). This equation shows that the mode rotation with $\omega > \omega_{cr}$ allows operation above the no-wall stability limit as long as this rotation is maintained. In addition to the rotating stable RWMs, the candidates to the fast RWMs described by (15.3) are also the saturated long-lived tearing modes. The examples are the $m/n = 2/1$ neoclassical tearing mode (NTM) rotating at 5–6 kHz in ASDEX Upgrade [149], $m/n = 3/2$ NTM with frequencies in the range 5–10 kHz in JT-60U [150], $m/n = 2/1$ mode rotating at 10 kHz in DIII-D [151]. Also, we can add to this group the fast rotating MHD instabilities (5–20 kHz) including NTMs in the NSTX spherical torus plasmas [152].

In tokamaks and stellarators, the most unstable are the modes with low n. In the reversed field pinches (RFPs), n is usually high and can play an important role in (18.2) which is equivalent to $n\omega_l\tau_w = 2r_w/d_w$. In the RFP device EXTRAP T2R, a tearing mode was observed with $m/n = 1/12$ and toroidal rotation frequency $\omega \approx 20$ krad s^{-1} [39]. It was concluded that the shell with $\tau_w \approx 8$ ms and $r_w/d_w = 198$ behaved almost like an ideal wall due to the fast mode rotation; the amplitude of the radial component of the core modes was very small at the shell [39]. The latter fact is consistent with (7.9), but this estimate does not yet justify the ideal wall model. With the mentioned wall time parameters, the mode is quantified by $n\omega\tau_w = 1920$.

https://doi.org/10.1017/S0022377815001403 Published online by Cambridge University Press

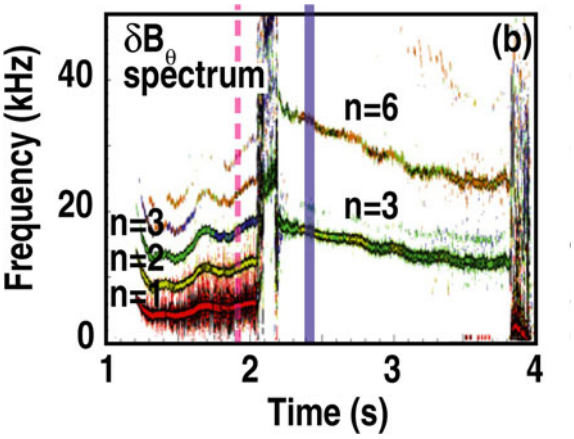


FIGURE 10. Coloured contour plot of the toroidal mode number, n, spectrum of magnetic fluctuations versus frequency and time. Vertical lines indicate times before and after the non-resonant magnetic field application in DIII-D tokamak. (Figure 4*b* from [160]. Figure courtesy by A. M. Garofalo.)

This means $\omega = 5\omega_l$, which is beyond ω_l, but not too far. From (13.5) we have $d_w/s = 2.2$ for this mode. Therefore, the resistive dissipation in the wall must give essential contribution to the rotational stabilization of such modes in the EXTRAP T2R.

In the TFTR tokamak, the observed magnetic perturbations with frequencies $\leqslant$30 kHz were called unusual as they did not always conform to expectations from MHD [153]. These perturbations were detected by an array of magnetic (Mirnov) coils located near the wall. Based on these facts, we can propose to consider the resistive wall effect on the modes as a possible reason for the 'unusual' behaviour.

We can add here such an interesting and still mysterious event as the appearance of edge harmonic oscillations (EHO) [154–164] observed on magnetic probes as a series of low-n harmonics with typically $n = 1$–4 the dominant component [159] or $n = 1$–6 [163]. In DIII-D, the EHO frequency detected on the magnetic probes was 6–10 kHz [154, 164] or 5–6 kHz in [160] that changed after the application of the $n = 3$ external perturbation, see figure 10. The measurements with beam emission spectroscopy at the plasma edge have shown similar oscillations at approximately 15 kHz in [162]. In the ASDEX Upgrade, the rotation frequency of the EHO was 7–11 kHz, while in JET the EHO fundamental frequency was approximately 15 kHz [155]. In NSTX, the coherent mode with characteristics similar to the EHO was observed at 2–5 kHz and lasted for several hundred milliseconds [161].

The EHO is usually described as a phenomenon accompanying the transition to the quiescent H-mode just below the ELM stability boundary. In our model, the EHO, being marginally stable, can be interpreted as a purely rotating mode with $\omega = \omega_{cr}$. We have $d_w/s = \sqrt{3}$ from (18.1) for 9 kHz and $\nu_l = 3$ kHz estimated for DIII-D. This proves that the skin effect is indeed essential for the observed EHOs and (15.3) could be applied to this case. In other words, the EHO can be explained as a mode which (marginal) stability is maintained by its interaction with the resistive wall.

In the existing models, the EHO is treated as a saturated kink/peeling or peeling-ballooning mode [157–164] destabilized by edge rotational shear [157, 161, 164]. Our analysis shows that destabilization of EHO must occur whenever the mode rotation frequency falls below the critical level. This can be easily tested in experiments as

https://doi.org/10.1017/S0022377815001403 Published online by Cambridge University Press

well as the prediction of (15.3) that increase of ω will make the EHOs more stable. Such testing will show whether or not the resistive wall affects the EHO dynamics. It will also be useful for selecting a better plasma model. The ideal MHD used in [157–164] gives $\omega = 0$ at the stability boundary [3–8], while our theory allowing for non-ideal effects shows that it must be finite $\omega = \omega_{cr}$ of the order of several kHz.

In experiments with the first observation of mode locking phenomena in LHD [165], the rotating $m/n = 1/1$ mode was continuously observed with a frequency of approximately 1.5–2 kHz. With estimated $\tau_w = 31.5$ ms and $r_w/d_w = 80$ [46], we have $\nu_l = 0.8$ kHz, which is a frequency when $d_w/s = 1$. Somewhat faster rotation of the mode in [165] means that our model of the rotational stabilization can be applicable to these events.

19. Precursors as fast RWMs

Equation (15.3) predicts that a rotationally stabilized mode becomes less stable at decreasing ω and, finally, unstable when the stability boundary $\omega = \omega_{cr}$ is crossed. With a destabilized slowly growing but still rotating perturbation, the braking torque on the plasma (proportional to $\omega \boldsymbol{b}^2$ [66, 91]) increases, which contributes to further decrease of ω and increase of γ_R. This must ultimately lead to mode locking, in which state the growth rate is largest at fixed g_R. This picture, based on (15.3), perfectly imitates the reality: in tokamaks, once a locked mode develops, the mode amplitude grows and the resulting high-amplitude saturated mode can degrade confinement quality or result in subsequent or immediate disruption [1]. Mode locking is a significant threat to the performance of next step tokamaks, but knowledge of the underlying physics is always claimed to be incomplete [1, 2]. In [1] it was stated that a mechanism responsible for the rapid growth of locked modes is not well understood. Our model suggests that an important part of the process must be the change of the energy dissipation in the wall when the mode evolves from the state with $\omega = \omega_{cr}$ to smaller ω and locking.

The mentioned frequency chirping at $\omega < \omega_{cr}$, the enhanced braking of the plasma rotation and increase of the growth rate are coupled by the 'positive feedback loop' through the growing perturbation amplitude. Simultaneous appearance of these effects in experiments on off-axis fishbone-like instability and excitation of RWMs in the DIII-D and JT-60U [25] are other examples where the model can be tested.

According to (15.3), the mode must be weakly damped when its rotation decreases to the critical level (or marginal stability) at $\omega = \omega_{cr}$. This formally corresponds to $g_R = g_I$ in (15.1) and (15.3). From this point, the plasma can either return back to a more stable state if it evolves to $g_R/g_I < 1$ or move to instability at $g_R/g_I > 1$ (for example, due to β rise or change in the pressure/current profiles). In the latter case, a mode continuous at $\omega = \omega_{cr}$ or slowly growing just after the transition to $\omega < \omega_{cr}$ will be a precursor to a more severe instability.

This is exactly what happens in the ELM cycle [1, 158, 166–173]. Various quasi-coherent (QC) modes in H-mode plasmas appear prior to the ELM and manifest themselves as periodical oscillations with increase in time amplitude (sometimes with slowdown in frequency) up to the ELM crash [167]. In TEXTOR, the QC modes observed with Mirnov coils were rotating with frequencies of 10 and 13.5 kHz [167]. Edge snakes and several types of the modes in a frequency range of several kHz in between type-I ELMs in the ASDEX Upgrade have been discussed in [169] (the vessel and the passive stabilizing loop were ignored in the simulation of the snake with a frequency about 2 kHz). A typical ELM signature on pickup coils measuring

https://doi.org/10.1017/S0022377815001403 Published online by Cambridge University Press

the radial magnetic field at ASDEX Upgrade is broadband, extending from a few kHz to several hundred kHz [171]. Type-I ELM precursors are often found in the frequency range 5–25 kHz in NSTX, and they are observable up to 200–500 μs preceding the ELM event [172].

In [173] it is reported that the type-I ELMs usually have an increased fluctuation level in the frequency band 25–50 kHz during the inter-ELM period for a few tens of ms before the ELM burst in the KSTAR tokamak. Such events with high enough mode rotation should be also analysed in terms of (15.3).

In tokamaks, the rotating ELM precursors grow on a ms time scale, whereas the non-rotating, or locked, precursors grow much faster, on a sub-ms scale [1]. Qualitatively, this is in excellent agreement with (15.3). In [1], a slower growth rate of the rotating precursors was attributed to the presence of some wall stabilization, and our model proves this suggestion and gives quantitative dependencies. An important point is that this must be not the ideal-, but the resistive-wall stabilization.

In the discussion of the ITER-related problems in [1], the magnetic precursors were considered as potentially having a causal relationship to, or acting as a trigger for, the ELM burst of magnetic fluctuations and transport. We would say that they rather act as an indicator of crossing the stability boundary at $\omega = \omega_{cr}$ and represent an initial stage of instability that becomes more violent at $\omega \ll \omega_{cr}$. Their analysis requires more careful description of the plasma–wall electromagnetic interaction with skin effect as a nonlinear regulator of the energy sink and braking torque.

The wall effect on the ELM dynamics is usually neglected and not even mentioned [163, 174]. This is an oversimplification, which can be proved by simple estimates of other kind. In the plasma–wall vacuum gap, the ELMs have a magnetic signature that differs from RWMs by higher m. In (9.4), the wall contribution with amplitude B^{out}_{mn} at the wall position ($x = 1$ at the wall) decreases as x^{m-1} towards the plasma, see (9.6). However, even at $m = 11$ it can be large enough at the plasma edge because $0.9^{10} \approx 0.35$ and $0.8^{10} \approx 0.1$. These two numbers compared to $0.7^{10} \approx 0.03$ also show that the $m = 11$ harmonic of $\boldsymbol{b}^w$ cannot strongly affect the inner region, but with the plasma–wall gap as narrow as $0.1r_w$ even the modes with larger m can experience wall stabilization (because $0.9^{20} \approx 0.1$). Comparison of high-m rotating edge modes with low-m RWMs is presented in [130].

These estimates show that existing theories of ELMs may undervalue a stabilizing role of the wall assuming 'the wall at infinity'. It is known that the RMP influence on the ELM behaviour is essentially different in different devices, which fact is not yet explained [175]. Proper account of the resistive wall effects, as described above, will be a natural (and necessary) step in resolving the uncertainties and contradictions.

There are also sawtooth or disruption precursors [1, 2, 7, 176–178]. In low beta JT-60U reversed shear plasmas, a growing precursor of magnetic fluctuation with a low frequency of ∼2.5 kHz was observed before disruption [177]. In the DIII-D, a major disruption was preceded by the growing $n = 1$ precursor oscillation measured by an external Mirnov loop [176]. Its frequency was 10–12 kHz, which falls into the 'fast RWMs' range. Mode locking is known to be an important aspect of the final phase of disruption precursor development [1]. This again points out the importance of the resistive wall stabilization in such cases.

20. Conclusion

The traditional theory of plasma stability against RWMs assumes $\boldsymbol{n} \cdot \boldsymbol{b}$ constant across the wall or $s \gg d_w$ thereby separating itself by a wide gap from the opposite

https://doi.org/10.1017/S0022377815001403 Published online by Cambridge University Press

'ideal wall' limit with $\boldsymbol{n} \cdot \boldsymbol{b} = 0$ and $s = 0$. This intermediate region under $s/d_w = 1$ corresponds to the modes faster than conventional RWMs but slower than the ideal MHD modes. Such 'fast RWMs' of various origin are often observed in tokamaks and stellarators, which is a good reason for developing an approach with realistic boundary conditions at the wall that allow for the skin effect to be taken into account. The result expressed by (15.3) shows that this is not a would-be-nice situation, but a necessity if we need a theory for a plasma stable above the no-wall ideal MHD limit.

With a strong skin effect, the wall acts as a magnetically thick conductor, effectively reducing the outer volume for the energy sink. As a consequence, a given energy flux into the wall is achieved at a larger growth rate γ_R of the locked modes than predicted by thin-wall models. The difference is described by (8.8) and (8.9) and illustrated by figure 5.

Calculations with and without a skin effect give the same stability boundary for the locked modes, but it is essentially different if the mode rotates fast enough. The mode rotation makes larger the induced electric field $\boldsymbol{E}$ and resistive losses of energy in the wall (because $\boldsymbol{\nabla} \times \boldsymbol{E} = -\partial \boldsymbol{b}/\partial t$). Affecting the energy balance, it suppresses γ_R as described by (15.3) valid for the fast RWMs and shown in figure 8. This favourable dependence of γ_R on ω, when the thin-wall model indicates independence, is the most dramatic difference in predictions of the two approaches, with and without the skin effect.

The rotational stabilization predicted by (15.3) must be robust and reliable because it is based upon the plasma–wall electromagnetic interaction and requires only the mode rotation with $\omega\tau_{sk} > 1$ (full stabilization is achieved at $\omega > \omega_{cr}$). Estimates show that the observed kink modes, tearing modes, EHOs and precursors of various instabilities can belong to this class. In particular, this effect can play a role in the disruption- and ELM-related events.

Incorporation of the skin effect into the existing stability theory can essentially improve its predictive capabilities and allow better discrimination between different plasma models.

Acknowledgements

The author is grateful to the participants of the ITPA Topical Group on MHD Stability for sharing the information and opinions over many years, to A. B. Mikhailovskii and V. S. Mukhovatov for inspiring this research, to Yu. V. Gribov, N. V. Ivanov and S. V. Konovalov for continuous support. Discussions and collaboration with F. Villone, V. V. Yanovskiy and Y. Q. Liu are greatly appreciated. Special gratitude to K. Yamazaki for suggesting the idea of this review. This work was supported by the Kurchatov Institute and National Research Nuclear University 'MEPhI'.

REFERENCES

[1] ITER Physics Expert Group on Disruptions Plasma Control and MHD and ITER Physics Basis Editors 1999 Chapter 3: MHD stability, operational limits and disruptions. *Nucl. Fusion* **39**, 2251–2389.

[2] Hender, T. C., Wesley, J. C, Bialek, J., Bondeson, A., Boozer, A. H., Buttery, R. J., Garofalo, A., Goodman, T. P., Granetz, R. S., Gribov, Y. *et al.* 2007 Chapter 3: MHD stability, operational limits and disruptions. *Nucl. Fusion* **47**, S128–S202.

[3] Bernstein, I. B., Frieman, E. A., Kruskal, M. D. & Kulsrud, R. M. 1958 An energy principle for hydromagnetic stability problems. *Proc. R. Soc. Lond.* A **244**, 17–40.

https://doi.org/10.1017/S0022377815001403 Published online by Cambridge University Press

[**4**] KADOMTSEV, B. B. 1966 Hydromagnetic stability of a plasma. In *Reviews of Plasma Physics* (ed. M. A. Leontovich), vol. 2, p. 153. Consultants Bureau.
[**5**] FREIDBERG, J. P. 1987 *Ideal Magnetohydrodynamics*. Plenum.
[**6**] MIYAMOTO, K. 1997 *Fundamentals of Plasma Physics and Controlled Fusion*. Iwanami.
[**7**] WESSON, J. A. 2004 *Tokamaks*, 3rd edn. Clarendon.
[**8**] GOEDBLOED, J. P. & POEDTS, S. 2004 *Principles of Magnetohydrodynamics*. Cambridge University Press.
[**9**] MIKHAILOVSKII, A. B. 1998 *Instabilities in a Confined Plasma*. Institute of Physics Publishing.
[**10**] CHU, M. S. & OKABAYASHI, M. 2010 Stabilization of the external kink and the resistive wall mode. *Plasma Phys. Control. Fusion* **52**, 123001.
[**11**] GAROFALO, A. M., JENSEN, T. H., JOHNSON, L. C., LA HAYE, R. J., NAVRATIL, G. A., OKABAYASHI, M., SCOVILLE, J. T., STRAIT, E. J., BAKER, D. R., BIALEK, J. *et al.* 2002 Sustained rotational stabilization of DIII-D plasmas above the no-wall beta limit. *Phys. Plasmas* **9**, 1997–2005.
[**12**] STRAIT, E. J., BIALEK, J., BOGATU, N., CHANCE, M., CHU, M. S., EDGELL, D., GAROFALO, A. M., JACKSON, G. L., JENSEN, T. H., JOHNSON, L. C. *et al.* 2003 Resistive wall stabilization of high-beta plasmas in DIII-D. *Nucl. Fusion* **43**, 430–440.
[**13**] GAROFALO, A. M., JENSEN, T. H. & STRAIT, E. J. 2003 Analysis of stable resistive wall modes in a rotating plasma. *Phys. Plasmas* **10**, 4776–4783.
[**14**] CHU, M. S., BONDESON, A., CHANCE, M., LIU, Y. Q., GAROFALO, A. M., GLASSER, A. L., LA HAYE, R. J., LAO, L. L., NAVRATIL, G. A. *et al.* 2004 Modeling of feedback and rotation stabilization of the resistive wall mode in tokamaks. *Phys. Plasmas* **11**, 2497–2504.
[**15**] STRAIT, E. J., BIALEK, J. M., BOGATU, I. N., CHANCE, M. S., CHU, M. S., EDGELL, D. H., GAROFALO, A. M., JACKSON, G. L., JAYAKUMAR, R. J., JENSEN, T. H. *et al.* 2004 Resistive wall mode stabilization with internal feedback coils in DIII-D. *Phys. Plasmas* **11**, 2505–2513.
[**16**] LA HAYE, R. J., BONDESON, A., CHU, M. S., GAROFALO, A. M., LIU, Y. Q., NAVRATIL, G. A., OKABAYASHI, M., REIMERDES, H. & STRAIT, E. J. 2004 Scaling of the critical plasma rotation for stabilization of the $n = 1$ resistive wall mode (ideal kink) in the DIII-D tokamak. *Nucl. Fusion* **44**, 1197–1203.
[**17**] OKABAYASHI, M., BIALEK, J., BONDESON, A., CHANCE, M. S., CHU, M. S., GAROFALO, A. M., HATCHER, R., IN, Y., JACKSON, G. L., JAYAKUMAR, R. J. *et al.* 2005 Control of the resistive wall mode with internal coils in the DIII-D tokamak. *Nucl. Fusion* **45**, 1715–1731.
[**18**] STRAIT, E. J. 2005 Stability limits of high-beta plasmas in DIII-D. *Fusion Sci. Technol.* **48**, 864–874.
[**19**] TURNBULL, A. D., BRENNAN, D. P., CHU, M. S., LAO, L. L. & SNYDER, P. B. 2005 Theory and simulation basis for magnetohydrodynamic stability in DIII-D. *Fusion Sci. Technol.* **48**, 875–905.
[**20**] GAROFALO, A. M. 2005 Resistive wall mode stabilization studies at DIII-D. *Fusion Sci. Technol.* **48**, 918–930.
[**21**] REIMERDES, H., HENDER, T. C., SABBAGH, S. A., BIALEK, J. M., CHU, M. S., GAROFALO, A. M., GRYAZNEVICH, M. P., HOWELL, D. F., JACKSON, G. L., LA HAYE, R. J. *et al.* 2006 Cross-machine comparison of resonant field amplification and resistive wall mode stabilization by plasma rotation. *Phys. Plasmas* **13**, 056107.
[**22**] REIMERDES, H., GAROFALO, A. M., JACKSON, G. L., OKABAYASHI, M., STRAIT, E. J., CHU, M. S., IN, Y., LA HAYE, R. J., LANCTOT, M. J., LIU, Y. Q. *et al.* 2007 Reduced critical rotation for resistive-wall mode stabilization in a near-axisymmetric configuration. *Phys. Rev. Lett.* **98**, 055001.
[**23**] STRAIT, E. J., GAROFALO, A. M., JACKSON, G. L., OKABAYASHI, M., REIMERDES, H., CHU, M. S., FITZPATRICK, R., GROEBNER, R. J., IN, Y., LA HAYE, R. J. *et al.* 2007 Resistive wall mode stabilization by slow plasma rotation in DIII-D tokamak discharges with balanced neutral beam injection. *Phys. Plasmas* **14**, 056101.
[**24**] OKABAYASHI, M., BOGATU, I. N., CHANCE, M. S., CHU, M. S., GAROFALO, A. M., IN, Y., JACKSON, G. L., LA HAYE, R. J., LANCTOT, M. J., MANICKAM, J. *et al.* 2009 Comprehensive control of resistive wall modes in DIII-D advanced tokamak plasmas. *Nucl. Fusion* **49**, 125003.

https://doi.org/10.1017/S0022377815001403 Published online by Cambridge University Press

[25] Okabayashi, M., Matsunaga, G., Degrassie, J. S., Heidbrink, W. W., In, Y., Liu, Y. Q., Reimerdes, H., Solomon, W. M., Strait, E. J., Takechi, M. *et al.* 2011 Off-axis fishbone-like instability and excitation of resistive wall modes in JT-60U and DIII-D. *Phys. Plasmas* **18**, 056112.

[26] Kamada, Y., Barabaschi, P., Ishida, S., Ide, S., Lackner, K., Fujita, T., Bolzonella, T., Suzuki, T., Matsunaga, G., Yoshida, M. *et al.* 2011 Plasma regimes and research goals of JT-60SA towards ITER and DEMO. *Nucl. Fusion* **51**, 073011.

[27] Kamada, Y., Barabaschi, P. & Ishida, S. 2013 Progress of the JT-60SA project. *Nucl. Fusion* **53**, 104010.

[28] Sabbagh, S. A., Sontag, A. C., Bialek, J. M., Gates, D. A., Glasser, A. H., Menard, J. E., Zhu, W., Bell, M. G., Bell, R. E., Bondeson, A. *et al.* 2006 Resistive wall stabilized operation in rotating high beta NSTX plasmas. *Nucl. Fusion* **46**, 635–644.

[29] Sontag, A. C., Sabbagh, S. A., Zhu, W., Menard, J. E., Bell, R. E., Bialek, J. M., Bell, M. G., Gates, D. A., Glasser, A. H., Leblanc, B. P. *et al.* 2007 Investigation of resistive wall mode stabilization physics in high-beta plasmas using applied non-axisymmetric fields in NSTX. *Nucl. Fusion* **47**, 1005–1011.

[30] Takechi, M., Matsunaga, G., Aiba, N., Fujita, T., Ozeki, T., Koide, Y., Sakamoto, Y., Kurita, G., Isayama, A., Kamada, Y. & The JT-60 Team 2007 Identification of a low plasma-rotation threshold for stabilization of the resistive-wall mode. *Phys. Rev. Lett.* **98**, 055002.

[31] Zakharov, L. & Putvinskii, S. V. 1987 Effect of plasma rotation in a tokamak on the stabilizing effect of a conducting wall. *Sov. J. Plasma Phys.* **13**, 68.

[32] Bondeson, A. & Ward, D. J. 1994 Stabilization of external modes in tokamaks by resistive walls and plasma rotation. *Phys. Rev. Lett.* **72**, 2709–2712.

[33] Gimblett, C. G. & Hastie, R. J. 1999 The effect of rotation on the stability of Resistive Wall Modes in tokamaks. In *Theory of Fusion Plasmas*, pp. 319–332. Editrice Compositori.

[34] Gimblett, C. G. & Hastie, R. J. 2004 The interaction of error fields and resistive wall modes. *Phys. Plasmas* **11**, 1019–1027.

[35] Haney, S. W. & Freidberg, J. P. 1989 Variational methods for studying tokamak stability in the presence of a thin resistive wall. *Phys. Fluids* B **1**, 1637–1645.

[36] Betti, R. & Freidberg, J. P. 1995 Stability analysis of resistive wall kink modes in rotating plasmas. *Phys. Rev. Lett.* **74**, 2949–2952.

[37] Taylor, J. B., Connor, J. W., Gimblett, C. G., Wilson, H. R. & Hastie, R. J. 2001 Resistive wall modes and nonuniform wall rotation. *Phys. Plasmas* **8**, 4062–4072.

[38] Chu, M. S., Chan, V. S., Chance, M. S., Edgell, D. H., Garofalo, A. M., Glasser, A. H., Guo, S. C., Humphreys, D. A., Jensen, T. H., Kim, J. S. *et al.* 2003 Modelling of feedback and rotation stabilization of the resistive wall mode in tokamaks. *Nucl. Fusion* **43**, 196–201.

[39] Frassinetti, L., Brunsell, P. R. & Drake, J. R. 2009 Experiments and modelling of active quasi-single helicity regime generation in a reversed field pinch. *Nucl. Fusion* **49**, 075019.

[40] Igochine, V. 2015 Chapter 6 resistive wall mode (RWM). In *Active Control of Magneto-Hydrodynamic Instabilities in Hot Plasmas* (ed. V. Igochine), Springer Series on Atomic, Optical, and Plasma Physics, vol. 83, pp. 183–226. Springer.

[41] Bialek, J., Boozer, A. H., Mauel, M. E. & Navratil, G. A. 2001 Modeling of active control of external magnetohydrodynamic instabilities. *Phys. Plasmas* **8**, 2170–2180.

[42] Bondeson, A., Liu, Y. Q., Gregoratto, D., Fransson, C. M., Lennartson, B., Breitholtz, C., Gribov, Y. & Pustovitov, V. D. 2002 Physics and control of resistive wall modes. *Phys. Plasmas* **9**, 2044–2050.

[43] Chu, M. S., Chance, M. S., Glasser, A. H. & Okabayashi, M. 2003 Normal mode approach to modelling of feedback stabilization of the resistive wall mode. *Nucl. Fusion* **43**, 441–454.

[44] Medvedev, S. Yu. & Pustovitov, V. D. 2004 Modeling of the feedback stabilization of the resistive wall modes in a tokamak. *Plasma Phys. Rep.* **30**, 895–906.

https://doi.org/10.1017/S0022377815001403 Published online by Cambridge University Press

[**45**] MAUEL, M. E., BIALEK, J., BOOZER, A. H., CATES, C., JAMES, R., KATSURO-HOPKINS, O., KLEIN, A., LIU, Y., MAURER, D. A., MASLOVSKY, D. *et al.* 2005 Dynamics and control of resistive wall modes with magnetic feedback control coils: experiment and theory. *Nucl. Fusion* **45**, 285–293.

[**46**] CHU, M. S. & ICHIGUCHI, K. 2005 Effect of the resistive wall on the growth rate of weakly unstable external kink mode in general 3D configurations. *Nucl. Fusion* **45**, 804–813.

[**47**] LANCTOT, M. J., REIMERDES, H., GAROFALO, A. M., CHU, M. S., LIU, Y. Q., STRAIT, E. J., JACKSON, G. L., LA HAYE, R. J., OKABAYASHI, M., OSBORNE, T. H. *et al.* 2010 Validation of the linear ideal magnetohydrodynamic model of three-dimensional tokamak equilibria. *Phys. Plasmas* **17**, 030701.

[**48**] LANCTOT, M. J., REIMERDES, H., GAROFALO, A. M., CHU, M. S., HANSON, J. M., LIU, Y. Q., NAVRATIL, G. A., BOGATU, I. N., IN, Y. G., JACKSON, G. L. *et al.* 2011 Measurement and modeling of three-dimensional equilibria in DIII-D. *Phys. Plasmas* **18**, 056121.

[**49**] SHIRAISHI, J., AIBA, N., MIYATO, N. & YAGI, M. 2014 Effects of centrifugal modification of magnetohydrodynamic equilibrium on resistive wall mode stability. *Nucl. Fusion* **54**, 083008.

[**50**] CHU, M. S., GREENE, J. M., JENSEN, T. H., MILLER, R. L., BONDESON, A., JOHNSON, R. W. & MAUEL, M. E. 1995 Effect of toroidal plasma flow and flow shear on global magnetohydrodynamic MHD modes. *Phys. Plasmas* **2**, 2236–2241.

[**51**] TAYLOR, T. S., STRAIT, E. J., LAO, L. L., MAUEL, M., TURNBULL, A. D., BURRELL, K. H., CHU, M. S., FERRON, J. R., GROEBNER, R. J., LA HAYE, R. J. *et al.* 1995 Wall stabilization of high beta plasmas in DIII-D. *Phys. Plasmas* **2**, 2390–2396.

[**52**] HU, B., BETTI, R. & MANICKAM, J. 2005 Application of the low-frequency energy principle to wall modes. *Phys. Plasmas* **12**, 057301.

[**53**] HAM, C. J., GIMBLETT, C. G. & HASTIE, R. J. 2009 Rotational stabilization of the resistive wall mode by coupling to a dissipative rational surface. *Plasma Phys. Control. Fusion* **51**, 115010.

[**54**] HAM, C. J., GIMBLETT, C. G. & HASTIE, R. J. 2011 Analytical modelling of resistive wall mode stabilization by rotation in toroidal tokamak plasmas. *Plasma Phys. Control. Fusion* **53**, 025001.

[**55**] LIU, Y. Q., CHU, M. S., CHAPMAN, I. T. & HENDER, T. C. 2008 Toroidal self-consistent modeling of drift kinetic effects on the resistive wall mode. *Phys. Plasmas* **15**, 112503.

[**56**] LIU, Y. Q., CHU, M. S., CHAPMAN, I. T. & HENDER, T. C. 2009 Modelling resistive wall modes in ITER with self-consistent inclusion of drift kinetic resonances. *Nucl. Fusion* **49**, 035004.

[**57**] BERKERY, J. W., SABBAGH, S. A., REIMERDES, H., BETTI, R., HU, B., BELL, R. E., GERHARDT, S. P., MANICKAM, J. & PODESTÀ, M. 2010 The role of kinetic effects, including plasma rotation and energetic particles, in resistive wall mode stability. *Phys. Plasmas* **17**, 082504.

[**58**] HAO, G. Z., LIU, Y. Q., WANG, A. K., JIANG, H. B., LU, G., HE, H. D. & QIU, X. M. 2011 Stabilization of the resistive wall mode instability by trapped energetic particles. *Phys. Plasmas* **18**, 032513.

[**59**] REIMERDES, H., BERKERY, J. W., LANCTOT, M. J., GAROFALO, A. M., HANSON, J. M., IN, Y., OKABAYASHI, M., SABBAGH, S. A. & STRAIT, E. J. 2011 Evidence for the importance of trapped particle resonances for resistive wall mode stability in high beta tokamak plasmas. *Phys. Rev. Lett.* **106**, 215002.

[**60**] HAO, G. Z., WANG, A. K., LIU, Y. Q. & QIU, X. M. 2011 Effect of trapped energetic particles on the resistive wall mode. *Phys. Rev. Lett.* **107**, 015001.

[**61**] BERKERY, J. W., BETTI, R. & SABBAGH, S. A. 2011 Investigation of multiple roots of the resistive wall mode dispersion relation, including kinetic effects. *Phys. Plasmas* **18**, 072501.

[**62**] YADYKIN, D., LIU, Y. Q. & PACCAGNELLA, R. 2011 Effects of kinetic resonances on the stability of resistive wall modes in reversed field pinch. *Plasma Phys. Control. Fusion* **53**, 085024.

[**63**] HAO, G. Z., LIU, Y. Q., WANG, A. K. & QIU, X. M. 2012 Kinetic effects of trapped energetic particles on stability of external kink modes with a resistive wall. *Phys. Plasmas* **19**, 032507.

https://doi.org/10.1017/S0022377815001403 Published online by Cambridge University Press

[64] Wang, Z. R., Guo, S. C. & Liu, Y. Q. 2012 Drift kinetic effects on the resistive wall mode stability – comparison between reversed field pinches and tokamaks. *Phys. Plasmas* **19**, 072518.
[65] Pustovitov, V. D. 2012 Thick-wall effects in the theory of resistive wall modes. *Phys. Plasmas* **19**, 062503.
[66] Pustovitov, V. D. 2013 Thick-wall effects on the rotational stabilization of resistive wall modes in tokamaks. *Nucl. Fusion* **53**, 033001.
[67] Pustovitov, V. D. 2013 Energy approach to stability analysis of the locked and rotating resistive wall modes in tokamaks. *Plasma Phys. Rep.* **39**, 199–208.
[68] Strumberger, E., Merkel, P., Sempf, M. & Günter, S. 2008 On fully three-dimensional resistive wall mode and feedback stabilization computations. *Phys. Plasmas* **15**, 056110.
[69] Albanese, R., Liu, Y. Q., Portone, A., Rubinacci, G. & Villone, F. 2008 Coupling between a 3-D integral eddy current formulation and a linearized MHD model for the analysis of resistive wall modes. *IEEE Trans. Magn.* **44**, 1654–1657.
[70] Portone, A., Villone, F., Liu, Y., Albanese, R. & Rubinacci, G. 2008 Linearly perturbed MHD equilibria and 3D eddy current coupling via the control surface method. *Plasma Phys. Control. Fusion* **50**, 085004.
[71] Villone, F., Liu, Y. Q., Paccagnella, R., Bolzonella, T. & Rubinacci, G. 2008 Effects of three-dimensional electromagnetic structures on resistive-wall-mode stability of reversed field pinches. *Phys. Rev. Lett.* **100**, 255005.
[72] Gribov, Y. & Pustovitov, V. D. 2002 Analytical study of RWM feedback stabilisation with application to ITER. In *Proceedings of the 19th IAEA Fusion Energy Conference (Lyon, 2002)*, IAEA. IAEA-CN-94/CT/P-12; http://www.iaea.org/programmes/ripc/physics/fec2002/html/fec2002.htm.
[73] Chance, M. S., Chu, M. S., Okabayashi, M. & Turnbull, A. D. 2002 Theoretical modelling of the feedback stabilization of external MHD modes in toroidal geometry. *Nucl. Fusion* **42**, 295–300.
[74] Pfirsch, D. & Tasso, H. 1971 A theorem on MHD-instability of plasmas with resistive walls. *Nucl. Fusion* **11**, 259–260.
[75] Reimerdes, H., Bialek, J., Chance, M. S., Chu, M. S., Garofalo, A. M., Gohil, P., In, Y., Jackson, G. L., Jayakumar, R. J., Jensen, T. H. *et al.* 2005 Measurement of resistive wall mode stability in rotating high-β DIII-D plasmas. *Nucl. Fusion* **45**, 368–376.
[76] Bondeson, A., Liu, Y. Q., Gregoratto, D., Gribov, Y. & Pustovitov, V. D. 2002 Active control of resistive wall modes in the large-aspect-ratio tokamak. *Nucl. Fusion* **42**, 768–779.
[77] Pustovitov, V. D. 2004 Error field amplification near the stability boundary of the modes interacting with a conducting wall. *Plasma Phys. Rep.* **30**, 187–195.
[78] Strumberger, E., Günter, S., Merkel, P., Riondato, S., Schwarz, E., Tichmann, C. & Zehrfeld, H. P. 2005 Numerical MHD stability studies: toroidal rotation, viscosity, resistive walls and current holes. *Nucl. Fusion* **45**, 1156–1167.
[79] Pustovitov, V. D. 2008 General formulation of the resistive wall mode coupling equations. *Phys. Plasmas* **15**, 072501.
[80] Pustovitov, V. D. 2012 Energy approach to the problem of plasma stability in tokamaks with a resistive wall. *Phys. Lett.* A **376**, 2001–2003.
[81] Pustovitov, V. D. 2012 A unified approach to description of the fast and slow resistive wall modes in tokamaks. *Plasma Phys. Rep.* **38**, 697–707.
[82] Katsuro-Hopkins, O., Sabbagh, S. A., Bialek, J. M., Park, H. K., Bak, J. G., Chung, J., Hahn, S. H., Kim, J. Y., Kwon, M., Lee, S. G. *et al.* 2010 Equilibrium and global MHD stability study of KSTAR high beta plasmas under passive and active mode control. *Nucl. Fusion* **50**, 025019.
[83] Manickam, J., Chance, M. S., Jardin, S. C., Kessel, C., Monticello, D., Pomphrey, N., Reiman, A., Wang, C. & Zakharov, L. E. 1994 The prospects for magnetohydrodynamic stability in advanced tokamak regimes. *Phys. Plasmas* **1**, 1601–1605.
[84] Pustovitov, V. D. 2009 Resistive ferromagnetic wall modes in theory and experiment. *Phys. Plasmas* **16**, 052503.

https://doi.org/10.1017/S0022377815001403 Published online by Cambridge University Press

[**85**] PUSTOVITOV, V. D. & VILLONE, F. 2010 Effect of ferromagnetic structures on RWM growth rates: a cylindrical model and a verification on JET. *Plasma Phys. Control. Fusion* **52**, 065010.

[**86**] PUSTOVITOV, V. D. & YANOVSKIY, V. V. 2015 Rotational stabilization of the resistive wall modes in tokamaks with a ferritic wall. *Phys. Plasmas* **22**, 032509.

[**87**] LEVESQUE, J. P., HUGHES, P. E., BIALEK, J., BYRNE, P. J., MAUEL, M. E., NAVRATIL, G. A., PENG, Q., RHODES, D. J. & STOAFER, C. C. 2015 Active and passive kink mode studies in a tokamak with a movable ferromagnetic wall. *Phys. Plasmas* **22**, 056102.

[**88**] ZHENG, L.-J. & KOTSCHENREUTHER, M. T. 2005 Wall thickness effect on the resistive wall mode stability in toroidal plasmas. *Phys. Plasmas* **12**, 072504.

[**89**] PUSTOVITOV, V. D. & YANOVSKIY, V. V. 2007 Dependence of the resistive wall mode growth rate on the wall thickness. In *Proceedings of the 34th EPS Conference on Plasma Phys (Warsaw, Poland, 2007)* vol. 31F (EPS, Mulhouse 2007) Paper P4.115.

[**90**] PUSTOVITOV, V. D. & MAYOROVA, M. S. 2006 Feedback stabilization of RWM with in-vessel coils. *Plasma Phys. Control. Fusion* **48**, 51–59.

[**91**] PUSTOVITOV, V. D. 2009 The rotating wall effect on the error field induced torque and the error field shielding in tokamaks. *Nucl. Fusion* **49**, 045003.

[**92**] PUSTOVITOV, V. D. 2011 Integral torque balance in tokamaks. *Nucl. Fusion* **51**, 013006.

[**93**] PUSTOVITOV, V. D. 2007 Dynamic diagnostics of the error fields in tokamaks. *Nucl. Fusion* **47**, 563–571.

[**94**] PUSTOVITOV, V. D. 2008 Decoupling in the problem of tokamak plasma response to asymmetric magnetic perturbations. *Plasma Phys. Control. Fusion* **50**, 105001.

[**95**] PUSTOVITOV, V. D. 2011 The linear model and experimentally observed resonant field amplification in tokamaks and reversed field pinches. *Plasma Phys. Rep.* **37**, 35–42.

[**96**] PUSTOVITOV, V. D. 2007 Rotational stabilization in the Boozer model. *Phys. Plasmas* **14**, 022501.

[**97**] BOOZER, A. H. 1999 Feedback equations for the wall modes of a rotating plasma. *Phys. Plasmas* **6**, 3180–3187.

[**98**] BOOZER, A. H. 2004 Robust feedback systems for resistive wall modes. *Phys. Plasmas* **11**, 110–114.

[**99**] FITZPATRICK, R. & AYDEMIR, A. Y. 1996 Stabilization of the resistive shell mode in tokamaks. *Nucl. Fusion* **36**, 11–38.

[**100**] PUSTOVITOV, V. D. 2007 Rotation and plasma stability in the Fitzpatrick–Aydemir model. *Phys. Plasmas* **14**, 082506.

[**101**] LIU, Y. Q., KIRK, A. & NARDON, E. 2010 Full toroidal plasma response to externally applied nonaxisymmetric magnetic fields. *Phys. Plasmas* **17**, 122502.

[**102**] TURNBULL, A. D. 2012 Plasma response models for non-axisymmetric perturbations. *Nucl. Fusion* **52**, 054016.

[**103**] WADE, M. R., NAZIKIAN, R., BATTAGLIA, D., BUTTERY, R. J., DEGRASSIE, J. S., EVANS, T. E., FENSTERMACHER, M. E., FERRARO, N. M., GRIERSON, B. A., HANSEN, J. M. *et al.* 2012 Advances in the physics understanding of ELM suppression using resonant magnetic perturbations in DIII-D. In *Proceedings of the 24th IAEA Fusion Energy Conference (San Diego, USA, 2012)*, IAEA. Paper EX/3-1.

[**104**] REIMAN, A., FERRARO, N. M., TURNBULL, A., PARK, J. K., CERFON, A., EVANS, T. E., LANCTOT, M. J., LAZARUS, E. A., LIU, Y., MCFADDEN, G. *et al.* 2015 Tokamak plasma high field side response to an $n = 3$ magnetic perturbation: a comparison of 3D equilibrium solutions from seven different codes. *Nucl. Fusion* **55**, 063026.

[**105**] OKABAYASHI, M., BIALEK, J., CHANCE, M., CHU, M. S., FREDRICKSON, E. D., GAROFALO, A. M., GRYAZNEVICH, M., HATCHER, R. E., JENSEN, T. H., JOHNSON, L. C. *et al.* 2001 Active feedback stabilization of the resistive wall mode on the DIII-D device. *Phys. Plasmas* **8**, 2071–2082.

[**106**] BARUZZO, M., BOLZONELLA, T., LIU, Y. Q., MANDUCHI, G., MARCHIORI, G., SOPPELSA, A., TAKECHI, M. & VILLONE, F. 2012 RWM control studies on RFX-mod with a limited set of active coils. *Nucl. Fusion* **52**, 103001.

https://doi.org/10.1017/S0022377815001403 Published online by Cambridge University Press

[107] Chapman, I. T., Hender, T. C., Howell, D. F., Erents, S. K., Gryaznevich, M. P., Shibaev, S., Stamp, M. F., De La Luna, E., Savchkov, A., Scannell, R. & The MAST Team & JET EFDA Contributors 2007 Perturbation of tokamak magnetic surfaces by applied toroidally asymmetric magnetic fields. *Nucl. Fusion* **47**, L36–L40.

[108] Liu, Y. Q., Chu, M. S., Guo, W. F., Villone, F., Albanese, R., Ambrosino, G., Baruzzo, M., Bolzonella, T., Chapman, I. T., Garofalo, A. M. *et al.* 2010 Resistive wall mode control code maturity: progress and specific examples. *Plasma Phys. Control. Fusion* **52**, 104002.

[109] Shafranov, V. D. & Zakharov, L. E. 1972 Use of the virtual-casing principle in calculating the containing magnetic field in toroidal plasma systems. *Nucl. Fusion* **12**, 599–601.

[110] Hirshman, S. P., Lazarus, E. A., Hanson, J. D., Knowlton, S. F. & Lao, L. L. 2004 Magnetic diagnostic responses for compact stellarators. *Phys. Plasmas* **11**, 595–603.

[111] Merkel, P. 1986 An integral equation technique for the exterior and interior Neumann problem in toroidal regions. *J. Comput. Phys.* **66**, 83–98.

[112] Gryaznevich, M. P., Liu, Y. Q., Hender, T. C., Howell, D. F., Beurskens, M., Chapman, I. T., Challis, C. D., Joffrin, E., Koslowski, H. R., Buratti, P., Solano, E. & JET-EFDA Contributors 2012 Determination of plasma stability using resonant field amplification in JET. *Nucl. Fusion* **52**, 083018.

[113] Schaffer, M. J., Snipes, J. A., Gohil, P., De Vries, P., Evans, T. E., Fenstermacher, M. E., Gao, X., Garofalo, A. M., Gates, D. A., Greenfield, C. M. *et al.* 2011 ITER test blanket module error field simulation experiments at DIII-D. *Nucl. Fusion* **51**, 103028.

[114] Pustovitov, V. D. & Yanovskiy, V. V. 2013 Analysis of the dispersion relation for resistive wall modes in tokamaks with account of the skin effect. *Plasma Phys. Rep.* **39**, 345–353.

[115] Pustovitov, V. D. & Yanovskiy, V. V. 2013 Modeling of the rotational stabilization of tokamak plasmas with account of skin effect in the resistive wall. *Plasma Phys. Rep.* **39**, 779–786.

[116] Villone, F. & Pustovitov, V. D. 2013 Skin effect modifications of the resistive wall mode dynamics in tokamaks. *Phys. Lett.* A **377**, 2780–2784.

[117] Sakasai, A., Masaki, K., Shibama, Y. K., Sakurai, S., Hayashi, T., Nakamura, S., Ozaki, H., Yokoyama, K., Seki, Y., Shibanuma, K. & The JT-60SA Team 2012 Manufacturing and development of JT-60SA vacuum vessel and divertor. In *Proceedings of the 24th IAEA Fusion Energy Conference (San Diego, USA, 2012)*, IAEA. Paper FTP/P7-20; www-naweb.iaea.org/napc/physics/FEC/FEC2012/html/proceedings.pdf.

[118] Liu, Y. Q., Chapman, I. T., Chu, M. S., Reimerdes, H., Villone, F., Albanese, R., Ambrosino, G., Garofalo, A. M., Gimblett, C. G., Hastie, R. J. *et al.* 2009 Progress in physics and control of the resistive wall mode in advanced tokamaks. *Phys. Plasmas* **16**, 056113.

[119] Strauss, H. R., Paccagnella, R. & Breslau, J. 2010 Wall forces produced during ITER disruptions. *Phys. Plasmas* **17**, 082505.

[120] Baruzzo, M., Bolzonella, T., Guo, S. C., Liu, Y. Q., Marchiori, G., Paccagnella, R., Soppelsa, A., Villone, F. & Wang, Z. R. 2011 3D effects on RWM physics in RFX-mod. *Nucl. Fusion* **51**, 083037.

[121] Villone, F., Chiariello, A. G., Mastrostefano, S., Pironti, A. & Ventre, S. 2012 GPU-accelerated analysis of vertical instabilities in ITER including three-dimensional volumetric conducting structures. *Plasma Phys. Control. Fusion* **54**, 085003.

[122] Jin, W., Ding, Y. H., Rao, B., Hu, Q. M., Jin, X. S., Wang, N. C., Zhang, X. Q., Wang, Z. J., Chen, Z. Y., Zhuang, G. & The J-Text Team 2013 Dependence of plasma responses to an externally applied perturbation field on MHD oscillation frequency on the J-TEXT tokamak. *Plasma Phys. Control. Fusion* **55**, 035010.

[123] Tsuzuki, K., Kamiya, K., Shinohara, K., Bakhtiari, M., Ogawa, H., Kurita, G., Takechi, M., Kasai, S., Sato, M., Kawashima, H. *et al.* 2006 Compatibility of reduced activation ferritic steel wall with high performance plasma on JFT-2M. *Nucl. Fusion* **46**, 966–971.

https://doi.org/10.1017/S0022377815001403 Published online by Cambridge University Press

[**124**] The JET Team, The JET Project – Design Proposal, Rep. EURJET-R5, CEC, Brussels (1975).
[**125**] BRUNSELL, P. R., KULDKEPP, M., MENMUIR, S., CECCONELLO, M., HEDQVIST, A., YADIKIN, D., DRAKE, J. R. & RACHLEW, E. 2006 Reversed field pinch operation with intelligent shell feedback control in EXTRAP T2R. *Nucl. Fusion* **46**, 904–913.
[**126**] CECCONELLO, M., MENMUIR, S., BRUNSELL, P. R. & KULDKEPP, M. 2006 Rotation in a reversed field pinch with active feedback stabilization of resistive wall modes. *Plasma Phys. Control. Fusion* **48**, 1311–1331.
[**127**] PUSTOVITOV, V. D. 2001 Feedback stabilization of resistive wall modes in a tokamak with a double resistive wall. *Plasma Phys. Rep.* **27**, 195–204.
[**128**] HUTCHINSON, I. H. 2001 Electromagnetic wall torques from magnetically confined plasmas. *Plasma Phys. Control. Fusion* **43**, 145–153.
[**129**] DEGTYAREV, L., MARTYNOV, A., MEDVEDEV, S., TROYON, E., VILLARD, L. & GRUBER, R. 1997 The KINX ideal MHD stability code for axisymmetric plasmas with separatrix. *Comput. Phys. Commun.* **103**, 10–27.
[**130**] PUSTOVITOV, V. D. & YANOVSKIY, V. V. 2014 Resistive wall stabilization of rotating edge modes in tokamaks. *Plasma Phys. Control. Fusion* **56**, 035003.
[**131**] PAZ-SOLDAN, C., BROOKHART, M. I., HEGNA, C. C. & FOREST, C. B. 2012 Wall-locking of kink modes in a line-tied screw pinch with a rotating wall. *Phys. Plasmas* **19**, 056104.
[**132**] ZHENG, L. J., KOTSCHENREUTHER, M. T. & VALANJU, P. 2014 Diamagnetic drift effects on the low-*n* magnetohydrodynamic modes at the high mode pedestal with plasma rotation. *Phys. Plasmas* **21**, 062502.
[**133**] MENARD, J. E., WANG, Z., LIU, Y., BELL, R. E., KAYE, S. M., PARK, J.-K. & TRITZ, K. 2014 Rotation and kinetic modifications of the tokamak ideal-wall pressure limit. *Phys. Rev. Lett.* **113**, 255002.
[**134**] DEGRASSIE, J. S. 2009 Tokamak rotation sources, transport and sinks. *Plasma Phys. Control. Fusion* **51**, 124047.
[**135**] CALLEN, J. D. 2011 Effects of 3D magnetic perturbations on toroidal plasmas. *Nucl. Fusion* **51**, 094026.
[**136**] CHAPMAN, I. T., LIU, Y. Q., ASUNTA, O., GRAVES, J. P., JOHNSON, T. & JUCKER, M. 2012 Kinetic damping of resistive wall modes in ITER. *Phys. Plasmas* **19**, 052502.
[**137**] WANG, Z. R., GUO, S. C., LIU, Y. Q. & CHU, M. S. 2012 Kinetic damping of resistive wall mode in reversed field pinch. *Nucl. Fusion* **52**, 063001.
[**138**] HAO, G. Z., LIU, Y. Q., WANG, A. K., MATSUNAGA, G., OKABAYASHI, M., MOU, Z. Z. & QIU, X. M. 2013 Destabilization of low-*n* peeling modes by trapped energetic particles. *Phys. Plasmas* **20**, 062502.
[**139**] CAI, H., CAO, J. & LI, D. 2014 The influence of energetic ions on resistive wall mode in reversed field pinch. *Nucl. Fusion* **54**, 032001.
[**140**] BERKERY, J. W., LIU, Y. Q., WANG, Z. R., SABBAGH, S. A., LOGAN, N. C., PARK, J.-K., MANICKAM, J. & BETTI, R. 2014 Benchmarking kinetic calculations of resistive wall mode stability. *Phys. Plasmas* **21**, 052505.
[**141**] LIU, Y. Q., CHAPMAN, I. T., GRAVES, J. P., HAO, G. Z., WANG, Z. R., MENARD, J. E., OKABAYASHI, M., STRAIT, E. J. & TURNBULL, A. 2014 Non-perturbative modelling of energetic particle effects on resistive wall mode: anisotropy and finite orbit width. *Phys. Plasmas* **21**, 056105.
[**142**] HE, Y., LIU, Y. Q., LIU, Y., HAO, G. & WANG, A. 2014 Plasma-resistivity-induced strong damping of the kinetic resistive wall mode. *Phys. Rev. Lett.* **113**, 175001.
[**143**] BERKERY, J. W., BETTI, R., SABBAGH, S. A., GUAZZOTTO, L. & MANICKAM, J. 2014 The effect of an anisotropic pressure of thermal particles on resistive wall mode stability. *Phys. Plasmas* **21**, 112505.
[**144**] GAROFALO, A. M., JACKSON, G. L., LA HAYE, R. J., OKABAYASHI, M., REIMERDES, H., STRAIT, E. J., FERRON, J. R., GROEBNER, R. J., IN, Y., LANCTOT, M. J. *et al.* 2007 Stability and control of resistive wall modes in high beta, low rotation DIII-D plasmas. *Nucl. Fusion* **47**, 1121–1130.

https://doi.org/10.1017/S0022377815001403 Published online by Cambridge University Press

[145] Mikhailovskii, A. B., Lominadze, J. G., Churikov, A. P. & Pustovitov, V. D. 2009 Progress in theory of instabilities in a rotating plasma. *Plasma Phys. Rep.* **35**, 273–314.

[146] Lepikhin, N. D. & Pustovitov, V. D. 2014 Dispersion relations for slow and fast resistive wall modes within the Haney–Freidberg model. *Phys. Plasmas* **21**, 042504.

[147] Pustovitov, V. D. 2015 Energy principle for the modes interacting with a resistive wall in toroidal systems. *Nucl. Fusion* **55**, 033008.

[148] Whyte, D. G., Hubbard, A. E., Hughes, J. W., Lipschultz, B., Rice, J. E., Marmar, E. S., Greenwald, M., Cziegler, I., Dominguez, A., Golfinopoulos, T. *et al.* 2010 I-mode: an H-mode energy confinement regime with L-mode particle transport in Alcator C-Mod. *Nucl. Fusion* **50**, 105005.

[149] García-Muñoz, M., Martin, P., Fahrbach, H.-U., Gobbin, M., Günter, S., Maraschek, M., Marrelli, L., Zohm, H. & The ASDEX Upgrade Team 2007 NTM induced fast ion losses in ASDEX upgrade. *Nucl. Fusion* **47**, L10–L15.

[150] Isayama, A., Oyama, N., Urano, H., Suzuki, T., Takechi, M., Hayashi, N., Nagasaki, K., Kamada, Y., Ide, S., Ozeki, T. & The JT-60 Team 2007 Stabilization of neoclassical tearing modes by electron cyclotron current drive in JT-60U. *Nucl. Fusion* **47**, 773–782.

[151] Van Zeeland, M. A., Yu, J. H., Chu, M. S., Burrell, K. H., La Haye, R. J., Luce, T. C., Nazikian, R., Solomon, W. M. & West, W. P. 2008 Tearing mode structure in the DIII-D tokamak through spectrally filtered fast visible bremsstrahlung imaging. *Nucl. Fusion* **48**, 092002.

[152] Menard, J. E., Bell, R. E., Gates, D. A., Gerhardt, S. P., Park, J.-K., Sabbagh, S. A., Berkery, J. W., Egan, A., Kallman, J., Kaye, S. M. *et al.* 2010 Progress in understanding error-field physics in NSTX spherical torus plasmas. *Nucl. Fusion* **50**, 045008.

[153] Takahashi, H., Fredrickson, E. D. & Chance, M. S. 2002 Unusual low frequency magnetic perturbations in the TFTR tokamak. *Nucl. Fusion* **42**, 448–485.

[154] Burrell, K. H., Austin, M. E., Brennan, D. P., Deboo, J. C., Doyle, E. J., Fenzi, C., Fuchs, C., Gohil, P., Greenfield, C. M., Groebner, R. J. *et al.* 2001 Quiescent double barrier high-confinement mode plasmas in the DIII-D tokamak. *Phys. Plasmas* **8**, 2153–2162.

[155] Suttrop, W., Hynönen, V., Kurki-suonio, T., Lang, P. T., Maraschek, M., Neu, R., Stäbler, A., Conway, G. D., Hacquin, S., Kempenaars, M. *et al.* 2005 Studies of the 'Quiescent H-mode' regime in ASDEX upgrade and JET. *Nucl. Fusion* **45**, 721–730.

[156] Oyama, N., Gohil, P., Horton, L. D., Hubbard, A. E., Hughes, J. W., Kamada, Y., Kamiya, K., Leonard, A. W., Loarte, A., Maingi, R. *et al.* 2006 Pedestal conditions for small ELM regimes in tokamaks. *Plasma Phys. Control. Fusion* **48**, A171–A181.

[157] Snyder, P. B., Burrell, K. H., Wilson, H. R., Chu, M. S., Fenstermacher, M. E., Leonard, A. W., Moyer, R. A., Osborne, T. H., Umansky, M., West, W. P. *et al.* 2007 Stability and dynamics of the edge pedestal in the low collisionality regime: physics mechanisms for steady-state ELM-free operation. *Nucl. Fusion* **47**, 961–968.

[158] Oyama, N. 2008 Progress and issues in understanding the physics of ELM dynamics, ELM mitigation, and ELM control. *J. Phys.: Conf. Ser.* **123**, 012002.

[159] Osborne, T. H., Snyder, P. B., Burrell, K. H., Evans, T. E., Fenstermacher, M. E., Leonard, A. W., Moyer, R. A., Schaffer, M. J. & West, W. P. 2008 Edge stability of stationary ELM-suppressed regimes on DIII-D. *J. Phys.: Conf. Ser.* **123**, 012014.

[160] Garofalo, A. M., Solomon, W. M., Park, J.-K., Burrell, K. H., Deboo, J. C., Lanctot, M. J., Mckee, G. R., Reimerdes, H., Schmitz, L., Schaffer, M. J. *et al.* 2011 Advances towards QH-mode viability for ELM-stable operation in ITER. *Nucl. Fusion* **51**, 083018.

[161] Sontag, A. C., Canik, J. M., Maingi, R., Manickam, J., Snyder, P. B., Bell, R. E., Gerhardt, S. P., Kubota, S., Leblanc, B. P., Mueller, D. *et al.* 2011 Pedestal characterization and stability of small-ELM regimes in NSTX. *Nucl. Fusion* **51**, 103022.

[162] Yan, Z., McKee, G. R., Groebner, R. J., Snyder, P. B., Osborne, T. H. & Burrell, K. H. 2011 High-frequency coherent edge fluctuations in a high-pedestal-pressure quiescent H-mode plasma. *Phys. Rev. Lett.* **107**, 055004.

https://doi.org/10.1017/S0022377815001403 Published online by Cambridge University Press

[**163**] SNYDER, P. B., OSBORNE, T. H., BURRELL, K. H., GROEBNER, R. J., LEONARD, A. W., NAZIKIAN, R., ORLOV, D. M., SCHMITZ, O., WADE, M. R. & WILSON, H. R. 2012 The EPED pedestal model and edge localized mode-suppressed regimes: studies of quiescent H-mode and development of a model for edge localized mode suppression via resonant magnetic perturbations. *Phys. Plasmas* **19**, 056115.

[**164**] BURRELL, K. H., GAROFALO, A. M., SOLOMON, W. M., FENSTERMACHER, M. E., ORLOV, D. M., OSBORNE, T. H., PARK, J.-K. & SNYDER, P. B. 2013 Quiescent H-mode operation using torque from non-axisymmetric, non-resonant magnetic fields. *Nucl. Fusion* **53**, 073038.

[**165**] TAKEMURA, Y., SAKAKIBARA, S., NARUSHIMA, Y., OKAMOTO, M., WATANABE, K. Y., SUZUKI, Y., OHDACHI, S., IDA, K., YOSHINUMA, M., TANAKA, K. *et al.* 2012 Mode locking phenomena observed near the stability boundary of the ideal interchange mode of LHD. *Nucl. Fusion* **52**, 102001.

[**166**] NEUHAUSER, J., BOBKOV, V., CONWAY, G. D., DUX, R., EICH, T., GARCIA-MUNOZ, M., HERRMANN, A., HORTON, L. D., KALLENBACH, A., KALVIN, S. *et al.* 2008 Structure and dynamics of spontaneous and induced ELMs on ASDEX upgrade. *Nucl. Fusion* **48**, 045005.

[**167**] SOLDATOV, S., KRÄMER-FLECKEN, A., KANTOR, M., UNTERBERG, B., SUN, Y., VAN OOST, G., REITER, D. & THE TEXTOR TEAM 2010 Turbulence, flows and edge localized mode (ELM) dynamics in limiter H-mode plasmas in TEXTOR. *Plasma Phys. Control. Fusion* **52**, 085001.

[**168**] OYAMA, N., HAYASHI, N., AIBA, N., ISAYAMA, A., URANO, H., SAKAMOTO, Y., KAMADA, Y., TAKIZUKA, T. & THE JT-60 TEAM 2011 Characteristics and control of the type I edge localized mode in JT-60U. *Nucl. Fusion* **51**, 033009.

[**169**] SOMMER, F., GÜNTER, S., KALLENBACH, A., MARASCHEK, M., BOOM, J., FISCHER, R., HICKS, N., LUHMANN, N. C. JR, PARK, H. K., REITER, B. *et al.* & THE ASDEX UPGRADE TEAM 2011 Characterization and interpretation of the edge snake in between type-I edge localized modes at ASDEX upgrade. *Plasma Phys. Control. Fusion* **53**, 085012.

[**170**] JIANG, M., XU, G. S., XIAO, C., GUO, H. Y., WAN, B. N., WANG, H. Q., WANG, L., ZHANG, L., NAULIN, V., GAN, K. F. *et al.* 2012 Characteristics of edge-localized modes in the experimental advanced superconducting tokamak (EAST). *Plasma Phys. Control. Fusion* **54**, 095003.

[**171**] WENNINGER, R. P., ZOHM, H., BOOM, J. E., BURCKHART, A., DUNNE, M. G., DUX, R., EICH, T., FISCHER, R., FUCHS, C., GARCIA-MUNOZ, M. *et al.* 2012 Solitary magnetic perturbations at the ELM onset. *Nucl. Fusion* **52**, 114025.

[**172**] SECHREST, Y., MUNSAT, T., BATTAGLIA, D. J. & ZWEBEN, S. J. 2012 Two-dimensional characterization of ELM precursors in NSTX. *Nucl. Fusion* **52**, 123009.

[**173**] BAK, J. G., AHN, J.-W., KIM, H.-S., LEE, J. W., YOON, S. W., MAINGI, R., HAN, H. S., JEON, Y. M., ENGLAND, A. C., PARK, Y. S. *et al.* 2012 ELM and pedestal structure studies in KSTAR H-mode plasmas. In *Proceedings of the 24th IAEA Fusion Energy Conference (San Diego, USA, 2012)*, IAEA. Paper EX/P4-12.

[**174**] HUYSMANS, G. T. A., PAMELA, S., VAN DER PLAS, E. & RAMET, P. 2009 Non-linear MHD simulations of edge localized modes (ELMs). *Plasma Phys. Control. Fusion* **51**, 124012.

[**175**] FENSTERMACHER, M. E., BECOULET, M., CAHYNA, P., CANIK, J., CHANG, C. S., EVANS, T. E., GOHIL, P., KAYE, S., KIRK, A., LIANG, Y. *et al.* 2010 ELM control by resonant magnetic perturbations: overview of research by the PEP ITPA group. In *Proceedings of the 23th IAEA Fusion Energy Conference (Daejon, Korea, 2010)*, IAEA. Paper ITR/P1-30.

[**176**] CALLEN, J. D., HEGNA, C. C., RICE, B. W., STRAIT, E. J. & TURNBULL, A. D. 1999 Growth of ideal magnetohydrodynamic modes driven slowly through their instability threshold: application to disruption precursors. *Phys. Plasmas* **6**, 2963–2967.

[**177**] TAKECHI, M., FUJITA, T., ISHII, Y., OZEKI, T., SUZUKI, T., ISAYAMA, A. & THE JT-60 TEAM 2005 MHD instabilities leading to disruptions in low beta JT-60U reversed shear plasmas. *Nucl. Fusion* **45**, 1694–1699.

[**178**] PAPP, G., POKOL, G. I., POR, G., MAGYARKUTI, A., LAZÁNYI, N., HORVÁTH, L., IGOCHINE, V., MARASCHEK, M. & ASDEX UPGRADE TEAM 2011 Low frequency sawtooth precursor activity in ASDEX upgrade. *Plasma Phys. Control. Fusion* **53**, 065007.

https://doi.org/10.1017/S0022377815001403 Published online by Cambridge University Press